Empirical Star Formation Estimates

in Galaxy Evolution

by

Nityasri Mandyam Doddamane

A DISSERTATION SUBMITTED IN PARTIAL FULFILLMENT

OF THE REQUIREMENTS FOR THE DEGREE OF

DOCTOR OF PHILOSOPHY

DEPARTMENT OF PHYSICS

NEW YORK UNIVERSITY

MAY, 2019

_____

Michael R. Blanton

Abstract

One of the crucial unsolved puzzles in astronomy has been the question of how galaxies end the process of star formation. A key piece in this puzzle is figuring out how to robustly infer star formation rates and the cosmic star formation histories of galaxies from observed photometric and spectroscopic data. The star formation history of a galaxy is encoded in its spectrum, which can be thought of as a fingerprint of a galaxy. However, spectroscopic information is often unavailable as it is more expensive to obtain. And where available, it can be limited in terms of interpretability by the dependence on the fiber diameter used and the physical properties of the galaxy in question.

The class of techniques known as SED (Spectral Energy Distribution) fitting tackles this problem by inferring the spectrum of a galaxy from photometric and spectroscopic data. Over the last decade, SED-fitting methods have become increasingly more sophisticated both in terms of model predictions as well as accounting for effects of more complex physical mechanisms such as dust absorption/emission. Another significant development, has been the rapidly growing field of IFU (Integral Field Unit) spectroscopy with a view to obtaining spatially resolved spectra with high S/N ratio of galaxies. With the advent of ongoing surveys such as MaNGA (Mapping Nearby Galaxies at Apache Point Observatory), the largest IFU-based survey thus far, we are better poised to answer this question than ever

before.

In this dissertation, I examine these two techniques for estimating star formation histories. First, using data from NASA Sloan Atlas (NSA) catalog along with the Wide-field Infrared Survey (WISE), I compare star formation rates obtained from two different methods: one, a UV-to-IR SED fitting method that accounts for dust and the other, a purely UV photometry-based approach. Using galaxy environments as a third independent parameter, I find a population of dust obscured star formers that masquerade as much lower star formation galaxies when only UV-optical information is available, but which live in the same large scale environments as other star forming galaxies.

In the second part, I examine the robustness of star formation history measurements from one of the largest available and most influential catalogs available, the Sloan Digital Sky Survey (SDSS) Legacy Survey. This catalog is limited by the fact that it uses small aperture fibers (3 arcsecond diameter) to measure galaxies that can sometimes have much larger angular extent. Spatially resolved spectroscopy from MaNGA measures galaxies more completely, but for a much smaller sample. I use aperture measurements of key spectral indicators of age, stellar mass and star formation history such as the $H\delta_A$ absorption line index and the $D_n 4000$ break to quantify the effects of the small fiber aperture on the Legacy Survey sample results. From these results I show that biases exist in the measurements of stellar mass from the SDSS Legacy Survey, but that for most galaxies these biases are small.

Contents

Listing of figures

For Srikar.

Acknowledgments

Here's where I acknowledge a lot of people.

... As for me, nothing in the universe can be the same
if somewhere, no one knows where, a sheep we never
saw has or has not eaten a rose.... Look up at the sky.
Ask yourself, "Has the sheep eaten the flower or not?"
And you'll see how everything changes.... And no grown-
up will ever understand how such a thing could be so
important!

Antoine de Saint-Exupêry (The Little Prince)

0
Introduction

0.1 A Brief History of Galaxy Evolution

0.1.1 The Discovery of Galaxies

One of the momentous shifts in scientific thinking was the realization that our Sun might be one of many stars in the Universe. From this sprung the idea that perhaps the gravitationally bound system of stars, stellar remnants, gas and dust that the Sun is a part of is one

of many such structures known as galaxies. The bright band of stars and dust that we observe in the night sky, which we now know as our own galaxy, the Milky Way, has been a puzzling topic since ancient times. The Greek philosopher Democritus is known to have speculated that this might be a band of distant stars (Lynn, 1901) but the thought was left by the wayside with the advent of Aristotelian physics. The astronomers of medieval Islam, centuries later, also hypothesized that the Milky Way was made of many stars such as our own Sun. However, observational proof for this came only in the 17th century when the Italian astronomer, Galileo Galelei pointed his telescope at this band and confirmed that the Milky Way was indeed made up of a huge number of faint stars.

Since the debate on a geocentric versus heliocentric Universe was still ongoing, Galileo's observations weren't given credence until more than century later, during which time, the development of Keplerian orbital mechanics and Newtonian Theory of Gravitation had resulted in a successful explanation of the Solar System and its dynamics. The idea that the galaxy might be a rotating configuration of a huge number of stars held together by gravitational forces that contained smaller gravitationally bound configurations such as our Solar System was first theorized by the English astronomer, Thomas Wright, in 1750. On the heels of his observation that the faint (then so-called) "nebulae" observed might be distant galaxies that came out of "external creations", philosopher Immannuel Kant (Clerke, 2010) hypothesized the existence of many such "island Universes" and speculated that these could potentially form and evolve independently from our own, thus laying the underpinnings of the study of galaxy formation and evolution.

William Herschel, in the 1780s, surveyed the stars in the Milky Way in multiple directions and discovered that the density of stars was greater on one side than the other. One of the earliest catalogues of galaxy-like objects was developed by Charles Messier, also towards the end of the 18th century, following which William Herschel assembled a catalog of 5000 nebulae. In the 19th century, with advances in optics and instrumentation, the first telescope to distinguish between elliptical and spiral galaxies was built by Lord Rosse. Additionally, this telescope could resolve point sources within the nebulae, thus confirming that galaxies were indeed "island universes" as Wright and Kant had surmised.

In early 20th century, astronomers were beginning to get interested in the chemical composition of these nebulae and started recording their spectra. With the advent of Einstein's Special Theory of Relativity, one could calculate the radial velocity of a "nebula" based on how its spectrum is Doppler-shifted. And so it happened that the American astronomer, Vesto Slipher, became the first person to measure galactic redshifts in 1912. While studying the chemical composition of bright spiral nebulae, he noticed that they were all highly Doppler-shifted, with estimated radial velocities that were much higher than the velocities of stars in the Milky Way. He also noticed that there were more "red-shifted" (i.e. moving away from us) nebulae than "blue-shifted" ones, an observation that would later propel Edwin Hubble to propose that the Universe was expanding.

In the 1920s, a series of observations made by Edwin Hubble, Ernst Opik, etc., confirmed that Andromeda was not a part of the Milky Way and was a galaxy is its own right, thus effectively settling the "Great Debate" of the times and confirming that our galaxy was just one of many galaxies in the Universe. Georges Lemaítre, a Belgian physicist, predicted, on

theoretical grounds rooted in Einstein's General Theory of Relativity, that the redshifts of galaxies should increase with distance. In 1929, Edwin Hubble looked at the distances and velocities of 46 galaxies and observed the same (Hubble, 1929): that their radial velocities increased with distance from us, thus theorizing what we know today as Hubble's Law (or alternately, the Hubble-Lemaítre Law). Edwin Hubble further analyzed the morphologies of these galaxies and came up with the Hubble Sequence, a classification of galaxy morphology (Fig. 1). The Swiss astrophysicist, Fritz Zwicky, in 1933, while studying galaxy clusters, noticed that the orbits of the galaxies were not accounted for by the mass of its luminous components, leading him to believe that there must be some "missing" mass (Zwicky, 1937) that does not interact electromagnetically, thus remaining unseen and termed it *dunkle Materie*, i.e.,"dark matter".

Thus with the emergence of new theories of spacetime, an expanding Universe that (as it was termed later) began with a "big bang", the existence of matter that doesn't interact electromagnetically, the study of galaxies in the 1930s set in motion a paradigm shift for astronomy and cosmology. The new questions were: How were the earliest galaxies formed? What would explain the diversity in morphologies seen in galaxies today? Is the Universe set to expand indefinitely? What drives the expansion of the Universe? What is dark matter? If the Universe's origins were homogeneous, how do we explain the heterogenous nature of the populations of galaxies seen?

0.1.3 Galaxy Evolution and Cosmology

The explorations in the latter half of the 20th century confirmed a few of the hypotheses discussed above, along with answering a few of those questions. In the 1960s and 1970s,

Vera Rubin, Kent Ford, and Ken Freeman analyzed rotation curves of spiral galaxies and provided strong evidence for the existence of dark matter (Freeman, 1970). Rubin inferred that most galaxies contain around six times as much dark matter as visible mass (Rubin et al., 1980), thus placing new constraints on galaxy formation and evolution in the Universe.

The two predominant theories of the origin of the Universe were: the "Big Bang Theory", originally proposed by Georges Lemaítre, and the "Steady State Theory" (essentially an unchanging Universe whose density remains the same in spite of expansion due to continuous creation of matter) proposed by Fred Hoyle. However, with theories of Big Bang Nucleosynthesis (the $\alpha\beta\gamma$ paper; Alpher et al. 1948) that successfully explained how the elements of the of the Universe came to be formed after the Big Bang and radio source counts which were also correctly accounted for by the Big Bang Theory swung cosmologists to favor this over the Steady State Theory. The final nail in the coffin was the successful detection of the Cosmic Microwave Background (CMB), predicted by the Big Bang Theory (Penzias & Wilson, 1965). According to the Big Bang Theory, the early Universe cools from a very hot state and remains an ionized plasma for the first few hundred thousand years (until redshift $z \sim 1100$). The emission from this era should be a Planck spectrum of the plasma at about the time that hydrogen recombines, redshifted due to the universe's expansion since then. This model predicts a spectrum peaking at near microwave wavelengths today, and the CMB is indeed detectable as a very low energy radiation with a blackbody temperature of 3K.

The discovery of dark matter coupled with the confirmation of the Big Bang Theory necessitated a theory of dark matter that would successfully explain the observable Universe.

In the 1980s, competing theories of hot and cold dark matter (Davis et al., 1985) were proposed. Eventually the cold dark matter theories won out as their prediction of the anisotropies in the CMB (Peebles, 1982) were successfully verified by the Cosmic Background Explorer (COBE) probe (Smoot et al., 1992) in combination with other data sets.

Before the turn of the century, the remarkable discovery of the accelerating universe (Riess et al., 1998) resulted in the resurrection of Einstein's cosmological constant and effectively confirmed ΛCDM as the clear winner among the cold dark matter models. The Big Bang Theory, together with the ΛCDM model, forms much of the basis of modern cosmology and the foundations for theories of galaxy formation and evolution.

0.2 Galaxy Formation and Evolution

0.2.1 Structure Formation in the Universe

The current model of cosmology suggests that there was a single event, the so-called "Big Bang" which resulted in the appearance of expanding space-time containing radiation, followed by an exponential expansion of space known as cosmic inflation (Guth, 1981) which established the initial properties of the Universe as being homogeneous, isotropic and flat. Tiny perturbations in this early Universe are responsible for structure formation. Cosmic inflation also explains the fact that these tiny quantum fluctuations grow into slight ripples of over-density and under-density thus seeding the early stages of structure formation in the Universe.

From a predominantly radiation-dominated Universe, with expansion, the density of radiation drops steeply leading to a the matter-radiation equality at 50,000 years after the Big Bang. Since dark matter only interacts gravitationally, the dark matter ripples from the

fluctuations form compact structures more freely as they are not opposed by other forces such as radiation pressure.

About 380,000 years after the Big Bang, the expansion of the Universe resulted in a lowering of density as well as a cooling down of its temperature to a point where protons and electrons in this plasma soup start combining to form the neutral hydrogen. Electrons decouple from the photons (these decoupled photons are what we detect as the CMB today) and the baryonic matter is now free to collapse under gravity creating local over-densities.

As fluctuations continue to grow, ever larger scales enter the non-linear regime of structure formation where dense concentrations of matter (dark and baryonic alike) get progressively denser. Dark matter begins to collapse into structures known as halos, and baryons fall with the dark matter into these halos. These structures arrange themselves into gravitationally stable configurations, a process known as virialization. The result of this process gives rise to a Universe that resembles a web (the cosmic web) with sheets and filaments of dark matter, creating a skeletal backbone in which star formation and galaxy formation eventually occur.

Within the dark matter halos baryonic matter can, when it becomes dense enough, additionally lose energy by radiation and can sink further into regions of high over-density. The stars and galaxies have their origins in these structures and are the resulting of the cooling of baryons deep in the potential wells of dark matter halos.

While a short summary of how galaxies form would be that the collapse of baryonic matter within dark matter halos results in disk-like structures that then collapse on small scales to form stars, the mechanisms by which this happens is still a topic of debate among astrophysicists. While a top-down scenario, wherein disk galaxies were formed from the collapse

of a single large cloud of gas (Eggen et al., 1962), captures some stages of galaxy formation well, in fact both theory and observations suggest that galaxies grow hierarchically — small galaxies form and merge into larger ones — which complexifies the picture. Meanwhile, the overall efficiency with which baryons form stars depends strongly on the halo mass (e.g. Behroozi et al. 2010), peaking at masses similar to that of the Milky Way. As Somerville & Davé (2015) describe, this dependence probably arises from processes that suppress star formation at lower masses (perhaps due to supernova feedback) and at higher masses (perhaps due to feedback from accreting supermassive black holes).

Since we are limited in our observations by the fact that we cannot observe galaxies in a time-resolved fashion (the time scales are too long), theories regarding galaxy formation rely computational simulations that evolve the initial conditions to the present day. We can compare the galaxies at each epoch to the populations observed at different redshift, assuming large scale homogeneity. As Somerville & Davé (2015) describe, these simulations incorporate the physics of ΛCDM, magnetohydrodynamics, and gravitation. Additionally, these models need to account for a variety of processes on subresolution scales that involve star formation, stellar and AGN feedback, and gas cooling to be able to correctly predict the observed Universe.

Thus, there are still many questions to be answered including and not limited to: how and where the baryons collapse, how galactic disks stabilize, the drivers and mechanisms of galactic feedback and what ultimately causes the relative frequency of different galaxy types in the observable Universe. There are thus many holes in this narrative of galaxy formation and evolution and astronomers are working to bridge this gap in two main ways: from the observational side, this involves accurate measurements of galaxy properties across cosmic

Hubble Sequence

E0

E6

S0 Sa Sb Sc

Unbarred examples

Irregular

Barred examples
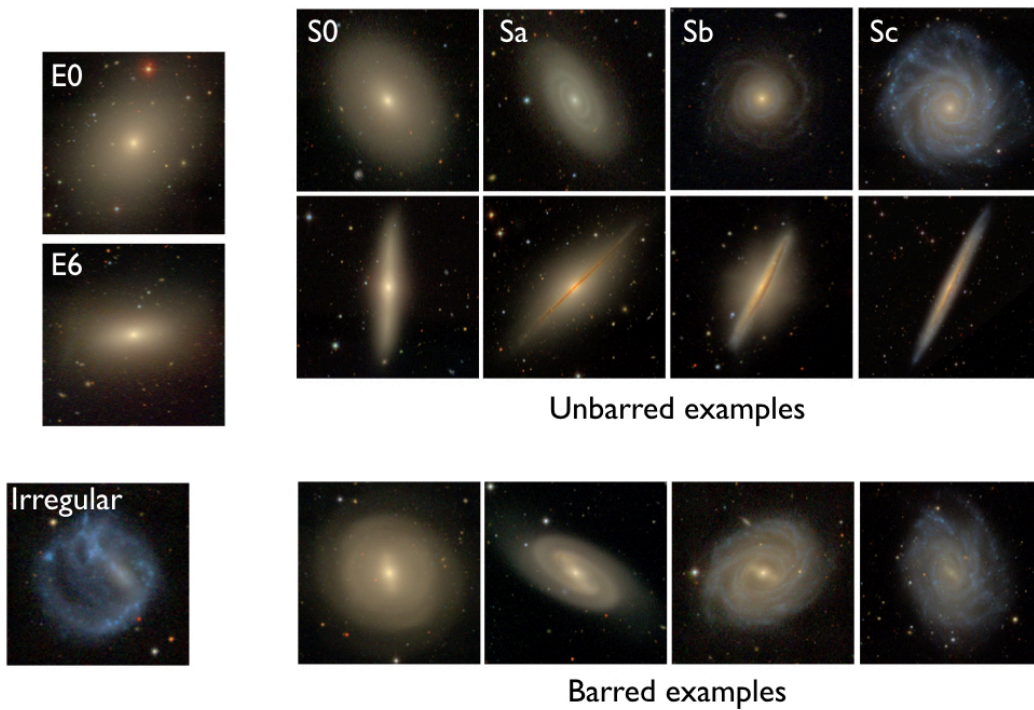
Figure 1: The Hubble Sequence: A classification scheme for galaxy morphologies (Photo credit: ?)

time and from the (theoretical) side of computational astrophysics, this involves fine-tuning the sub-grid models of galaxy formation and evolution simulations so as to be able to reproduce the estimated from the properties. These both take from and in turn inform the parameters in the ΛCDM model of the Universe that cosmologists are engaged in refining.

0.2.2 Galaxy Properties in the Observable Universe

The commonly used classification scheme for galaxies based on their most obvious attribute, the morphologies of their luminous components, was invented by Edwin Hubble in 1926. The classification scheme is based on the relative sizes and of the bulges and disks in galaxies and broadly encompasses four types of morphologies: elliptical, lenticular, spiral and irregular (Fig. 1). Galaxy morphologies are strongly correlated with their other physical properties such as luminosity, age, chemical composition, star formation histories and kinematics (Roberts & Haynes 1994). The bulges usually contain older, redder stars and the disks are characterized by mixed stellar populations along with gas and dust. The disks may also contain spiral arms which usually contain pockets of star formation activity. Elliptical galaxies have almost no disk. Lenticulars are smooth like ellipticals but contain a puffy, thick disk that when observed obliquely has a distinct oval-like appearance (lentil-shaped!). Spirals can have a bulge but are characterized by their thin disk, often with spiral arms. Irregulars are akin to spirals but as their name suggests, appear less organized in their light distribution. Early ideas about galaxy evolution suggested that galaxies formed as ellipticals or lenticulars (referred to as 'early-type' galaxies) and later evolved into spirals or irregulars (referred to as 'late-type' galaxies) and while there are strong correlations between galactic structure and their star formation rates, it is now known that this is in general untrue.

The total amount of light we observe emanating from a galaxy is the second obvious trait that lends itself to comparison. This can be quantified as "luminosity," the amount of energy emitted by a star per unit time, often measured in units of the solar luminosity $L_\odot$, and usually measured in a particular wavelength bandpass. Optical or near-infrared luminosity can serve as a reasonable (but not exact) proxy for stellar mass; ultraviolet luminosity can serve as a reasonable (but not exact) proxy for current star formation activity. Observations reveal that fainter galaxies are more frequent per unit volume than galaxies as bright as our own. Very bright big ellipticals are much rarer than both. The distribution of galaxy luminosities, per volume and per unit luminosity, is known as the "luminosity function" (Blanton et al. (2005); Efstathiou et al. (1988)), which provides key constraints on galaxy formation and evolution.

The total luminosity of a galaxy in the ultraviolet through near infrared is generally dominated by stars, and the stellar population is changing with time as stars evolve off the main sequence and reach their fates, for example as black holes, neutron stars, or white dwarfs. A more stable and sometimes more interesting quantity is the total mass in stars, the stellar mass. Because the luminosities of stars varies as $L \propto M^{-\alpha}$, where $\alpha \sim$ 3–5, and the more massive stars die rapidly, the total ratio of luminosity to stellar mass varies over time. Furthermore, because the massive stars are very hot, the overall color of the stellar population starts out blue and becomes increasing red. This pattern leads to a relationship between the galaxy spectrum and the stellar mass to light ratio, that can be exploited to estimate the stellar mass of a galaxy.

The most basic measure of the spectral energy distribution of galaxies are its colors. Colors in astronomy are defined on the basis of the ratios of observed fluxes in various band-

passes. For instance, $g - r$ is 2.5 $\log_{10}$ of the ratio of the r-band to g-band flux, where g and r are optical bandpasses used in the Sloan Digital Sky Survey (SDSS); larger $g - r$ indicates a redder galaxy. Galaxy populations have a bimodal distribution and can be divided into the so-called "red sequence" and "blue cloud" (Blanton et al. (2003); Strateva et al. (2001)). The blue cloud is dominated by star-forming blue spirals with young stellar populations; the red sequence has a mixture of varied populations, including some older or dust-reddened spirals, lenticular galaxies, and ellipticals. The intermediate colored population, the so-called "green valley", must contain (but does not only contain) the population of galaxies that are in the process of ending their star formation and transitioning from blue to red. However, a complication to this simple interpretation of the observations is the presence of dust, which has the tendency to make galaxies appear redder. We investigate the star formation of galaxies in the context of optical colors and dust, further in Chapter 1.

The last significant observable property we introduce here is the galaxy environment, which is a measure for each galaxy of how many other galaxies are nearby it relative to the mean galaxy density. Galaxies exhibit substantial clustering relative to a Poisson distribution, leading to a large dynamic range in local density For example, a galaxy like the Milky Way most commonly has not similarly massive neighbors within 1 Mpc, but massive clusters of galaxies have 100s of Milky Way-sized galaxies within a Mpc. This clustering of galaxies reveals information about cosmological parameters, like the initial amplitude of fluctuations and the mean dark matter density.

The environment of galaxies also appears to be correlated with their formation history, as manifested by their morphology (Dressler, 1980), luminosity (Norberg et al., 2002), star formation rates (Lewis et al., 2002), and numerous other properties. For instance, simplis-

tically, blue galaxies preferentially exist in isolated environments (or voids) and large red ellipticals preferentially exist in clusters. Galaxy environments can be measured in a variety of ways, such as counts in a projected aperture or distance to nearest neighbor (Cooper et al., 2005). The density field length scales at which galaxy environment matters significantly enough to affect its star formation has been investigated; it appears that the local environment (within 1–2 Mpc) is most important, with the larger scale environment being of much less importance at a fixed local environment (Blanton et al. (2006); Kauffmann et al. (2004); Park et al. (2007)).

0.2.3 Questions in Galaxy Evolution

The lifecycle of a galaxy can be thought of in terms of the timeline of the events between the formation of the first stars in the galaxy began to when there is little to no star formation activity in the galaxy, i.e. the galaxy is quenched. Many processes determine the history of star formation and how it may end. Star formation begins with the inflow of gas, its formation into galactic disk structures, its radiatively cooling, the formation of molecular clouds, and the formation of stars. The stars form in some initial mass distribution whose form in the Milky Way is constrained observationally, but whose variation among galaxies is largely unknown. The massive stars in the stellar mass distribution tend to disassociate and ionize the surrounding gas, dispersing the cloud that is forming stars. This feedback can even heat or remove surrounding gas clouds in the disk. Other feedback processes, such as accreting supermassive black holes at the centers of galaxies, can also remove gas and suppress star formation. For most massive galaxies, including the Milky Way, current star formation rates are rapid enough to consume the remaining gas in 2–3 billion years; this fact is

widely interpreted to indicate that to remain star forming, galaxies require a steady inflow of gas from the external environment.

Models of galaxy formation built from numerical hydrodynamic simulations (Crain et al. (2015); Davé et al. (2016); Sijacki et al. (2015)) are powerful enough now to predict this evolutionary process in a cosmological context. However, they can typically resolve scale of only 100 pc or so, which is far larger than a forming star or even an individual massive molecular cloud. The detailed star formation and feedback processes are therefore the product of subgrid physics (Agertz et al., 2007) that are calibrated on the observations themselves. There are a number of free parameters in the subgrid models, characterizing the rate of star formation as a function of local conditions, the effects of supernova (Creasey et al., 2013) and stellar feedback (Hopkins et al., 2012), the activity of supermassive black holes, and other effects. The calibration of the parameters used for these simulations, and the use of the simulations as a test of the overall picture for cosmological galaxy formation, therefore requires that the observations they are calibrated on and compared to are correct.

The stellar mass and star formation rates of galaxies represent a coupled pair of galaxy properties that are critical in this process. The stellar mass function (analogous to the luminosity function) has a shape very different than the halo mass function, with a shallow slope at the faint end and a steep cutoff at the bright end. This shape implies that star formation is suppressed at the highest masses, and also at low masses. The simulations generally explain these features using supermassive black hole feedback at high mass and supernova feedback at low mass. The degree and type of feedback required is determined by the observed stellar mass function.

The star formation patterns are also informative. For star-forming galaxies, the star for-

mation rates scale approximately as $M_*^{2/3}$ (Noeske et al., 2007). Fully quenched galaxies are found at the highest masses and/or in the densest regions. What determines the star formation rates, and what processes quench some galaxies, are important questions the simulations are designed to help answer. The simulation parameters can be tuned to produce these patterns, but the meaningfulness of those tuning parameters, and the legitimacy of additional predictions the simulations may make, depends on the reliability of the observations they are tuned to.

0.3 Observational Indicators of Star Formation and Stellar Mass

In this section we will review how astronomers observationally infer star formation rates and stellar masses in galaxies.

0.3.1 Integrated Star Formation Rates for Galaxies

Since we know that star formation ultimately is the result of the collapse within Giant Molecular Clouds (GMC) of cold gas, it follows that the star formation rate in a galaxy must relate to the availability of cold molecular gas. It was first proposed by Schmidt in 1959 (Schmidt, 1959) that star formation in a galaxy scales with the the surface density of gas in the galaxy. As reviewed by Kennicutt (1998), the mean surface density of galaxy star formation rate is approximately related to the mean surface density of the cold gas in the galaxy (neutral plus molecular gas) by a power law known as the Kennicutt-Schmidt Law:

$$\Sigma_{SF} = A\Sigma_g{}^N$$

The determination of N relies on a host of empirical studies based on gas content and star

formation from a host of disk and starburst galaxies and is found to be $\sim 1.3 - 1.5$. The neutral gas content is detected through emission from the 21 cm hyperfine transition of hydrogen, assuming a cosmic mean helium fraction. Molecular gas is dominated by H_2, which unfortunately does not have strong emission lines at typical molecular cloud temperatures. The molecular gas mass is typically inferred from trace molecules like CO and HCN.

To be able to infer star formation rates from galaxies, one has to investigate their stellar populations. As it is almost impossible to resolve stars in galaxies (barring the closest ones) even with space telescopes, to get the star formation properties of a galaxy, we rely on integrated light measurements in the Ultraviolet (UV) and Infrared (IR) continuum or the so-called nebular recombination lines. A comprehensive review of this subject can be found in Kennicutt & Evans (2012). For instance, because short-lived, massive stars have high temperatures at their surface, the continuum luminosity integrated across the blue or near-UV part of the spectrum is an indicator of recent star formation. The quantitative relationship between recent star formation and the UV light depends for its calibration on evolutionary synthesis models (Section 0.3.2) and an assumption about the stellar initial mass function (IMF), since the bulk of the stellar mass is in low mass stars, but the bulk of the light comes from the massive stars. For example, Madau et al. (1998) and Kennicutt & Evans (2012) report calibrations (assuming a Salpeter IMF; Salpeter 1955): relative to the UV Luminosity L (in a wavelength range of 1500 Å- 2800 Å):

$$\text{SFR} \left(M_\odot \text{yr}^{-1} \right) = 1.4 \times 10^{-28} L_\nu \left(\text{ergs s}^{-1} \right) \text{Hz}^{-1}$$

A significant issue with inferring a UV star formation rate is the presence of dust in galaxies. Dust absorbs a significant fraction of the bluer part of the spectrum, and because

of its low temperature re-emits the absorbed energy in the mid- and far-infrared. Any UV star formation measurement thus needs to account for this dust attenuation. Furthermore, because of these effects, the infrared light (10–100 μm) is a tracer of the star formation rate as well. we will discuss further these issues further in Chapter 1.

Star formation in galaxies, specifically the production of hot and massive stars, results in the heating and ionization of gas in the Interstellar Medium (ISM), which in turn leads to observable line emission. The most significant of these are the Balmer emission lines due to emission from Hydrogen during the recombination processes that balance the ionization processes in the nebulae surrounding hot stars. These nebulae are known as HII regions, and the presence of HII regions in a galaxy and their characteristic Balmer line emission is thus a probe of a young massive stellar population. The strongest of these recombination lines in the optical is the $n = 3$ to $n = 2$ transition, the $H\alpha$ line at 656.28nm. During the recombination process, electrons enter at typically high n states. following that event, any direct transition from some high n to the $n = 1$ state will lead to a photon which is quickly absorbed under nebular conditions by exciting another nearby atom. This resonant scattering continues under the photon is absorbed on dust, or a rare 2-photon decay occurs from the $2s$ state, or Doppler shifts scatter the photon into the wings of the absorption line. The net effect is that almost every ionizing photon leads to a Balmer photon. The ratio of the resulting Balmer lines to each other can be calculated and is relatively constant, with weak dependence on temperature or electron density. Thus, one of the most widely used estimators of SFR is a linear function of the emission line luminosity of the $H\alpha$ line (Kennicutt

et al. (1994); Madau et al. (1998)):

$$\mathrm{SFR}\ (\mathrm{M_\odot yr^{-1}}) = 7.9 \times 10^{42} \mathrm{L(H\alpha)\ (ergs\ s^{-1})}$$

The bluer Balmer emission lines such sa as *Hβ* are intrinsically weaker, and often substantially dust-reddened.

Collisionally excited lines such as the [OII] doublet at 3727 Å also correlate with star formation, but are much more sensitive to the metallicity, temperature, and density of the gas.

All the star formation rates discussed above assume some priors on the evolution of the galaxy from the IMF chosen to the timelines of starbursts and effective stellar population synthesis models are required to be able to successfully account for the spectral energy distribution of the galaxy and give accurate insights into the stellar and dust content of the galaxy.

0.3.2   SPECTRAL DIAGNOSTICS AND STELLAR POPULATION SYNTHESIS MODELS

The galaxy spectrum contains an imprint of its Star Formation History (SFH), stellar metallicity and abundance pattern, stellar Initial Mass Function (IMF), total stellar mass and the nature of its gas and dust content. However, to be able to interpret the details in a spectrum accurately, one has to rely on evolutionary synthesis models or what are called Stellar Population Synthesis (SPS) models. Typically these models contain a comprehensive library of stellar spectra of stars across ages, masses and luminosities. The earliest such models (Faber 1972; Spinrad & Taylor 1971) relied on using a linear combination of the diverse individual stellar spectra to reconstruct the integrated light emission from a galaxy. How-

ever, populations of stars do not come in arbitrary mixes — stars are formed together in groups that evolve over time in a regular way. More recent models (Bruzual & Charlot 2003a; Leitherer & Heckman 1995; Schulz et al. 2002) involve setting handful of global parameters, such as the IMF, the SFR, the rate of chemical enrichment, and using the laws of stellar evolution and of stellar atmospheres to predict the emergent integrated spectrum of the population as it evolves in time.

Broadly speaking, SPS models require the following ingredients (Walcher et al., 2011): an IMF, stellar evolutionary tracks (isochrones), stellar spectral libraries, and a SFR and chemical evolution model. The choice of IMF (Chabrier 2003; Kroupa 2001; Salpeter 1955) determines the distribution of stellar masses initially and the spectral libraries convert the stellar evolution outputs such as surface gravity and effective temperature into observable Spectral Energy Distributions (SEDs). The spectral libraries can either be calculated theoretically (Coelho et al. 2005; ?) or on a purely empirical basis and are oftentimes a combination of both. Some notable modern stellar spectral libraries constructed from observations are ELODIE (Prugniel & Soubiran, 2004), STELIB (Le Borgne et al., 2003), MILES (Sánchez-Blázquez et al., 2006), and most recently MaStar (Yan et al., 2018).

The next step in reconstructing the SED of a galaxy is to account for the effect of the Interstellar Medium (ISM) on the integrated light from the simple stellar population. The ISM primarily consists of gas and dust, and a model to account for the radiative transfer through the ISM is needed. Photoionization codes such as CLOUDY (Ferland et al., 2013) account for the ionization of atomic gas by star light and the resulting emission, most prominently the emission lines. The SED of both the stellar emission and the ISM emission is strongly affected by the dust intermixed in the gas, which redistributes energy via scat-

tering and absorption from the bluer part of the spectrum, re-emitting absorbed light in the infrared. Models of dust (Calzetti et al. 2007; Draine & Li 2007) are thus almost always combined with the SPS models.

The evolutionary synthesis models combined with the dust models can effectively predict a galaxy SED at any instant in its cosmic history as needed, thus enabling them to be able to be compared to photometric or spectroscopic data from galaxies at arbitrary redshifts. The method of fitting observed data using a SPS model to infer the physical properties of a galaxy is known as SED fitting. The input data can either be in the form of photometric broadband fluxes or observed spectra, either the full spectrum or specific measurements of the spectrum known as spectral indices. A recent review on the subject of SED fitting can be found in Conroy (2013).

SED fitting requires searching a large model space of the SPS and dust libraries and evaluating how well-matched to observations are the predicted SEDs for a chosen set of parameters relating to the SFH and dust attenuation. SED fitting codes employ a range of techniques, to perform this mimization; examples of these codes are MAGPHYS (da Cunha et al., 2008), CIGALE (Noll et al., 2009) and Prospector (Leja et al., 2017).

There are a couple of things worth noting about SED fitting. First, all the parameters except for the overall normalization are set by the "shape" of the spectrum, i.e., the observation flux ratios between photometric bandpasses ("colors") or spectral channels. Thus, parameters like the dust attenuation, metallicity, age of the stellar population, are independent of the bolometric luminosity. It is often convenient to derive parameters like the mass-to-light ratio (M/L) of the galaxy, the Specific Star Formation Rate (SSFR, the SFR per unit solar mass), dust attenuation, and metallicity. Secondly, the robustness of fitting

an SED to observed spectrometric and photometric data relies a lot on how the systematic uncertainties in the SPS (and dust) models are accounted for. Thus the priors on the SFH and dust libraries can significantly impact the inference of the stellar mass, SFR and mean stellar age.

0.3.3 Inferring M_* and SFR from SED fitting

As noted above, parameters of fundamental interest for galaxies are their stellar masses, or total amount of mass in stars within a galaxy (M_*), and their star formation rates. Both are estimated on the basis of SPS models. In the case of stellar mass, the SPS models predict SEDs that can be compared to observations. In the case of star formation, the SPS models predict the UV and ionizing spectrum of stellar populations. The UV light can be directly observed, supplemented with IR observations to quantify the UV light reprocessed by dust. The ionizing photons can be measured through emission lines from the ionized nebulae.

Photometry provides useful constraints on stellar mass. A useful concept in the quantification of stellar mass is that the Mass-to-Light ratio in some bandpass (M/L), from which the stellar mass can be obtained by multiplying the luminosity within the wavelength range under consideration. The simplest measures of M/L ratios involve using their relationships with color between a single pair of bandpasses (e.g. $g - r$ or $u - g$); generally speaking, the redder the color, the higher the M/L ratio. Bell & de Jong (2001) used the Bruzual & Charlot (2003a) SPS models to map the relationship between M/L and color as a function of metallicity and SFH. Zibetti et al. (2009) also later developed tables for the color-M/L relationship using a library of model galaxy SEDs. A related measure of stellar mass is by using

SED fitting methods on broadband photometry, that fit more than two bandpasses simultaneously. Of the physical parameters inferred via SED fitting, stellar masses tend to be relatively robust (Muzzin et al., 2009; Papovich et al., 2001), especially in comparison to SFR estimates. One reason for this is that the effect of dust-reddening, stellar age, and metallicity cause similar variations in the color-M/L plane. Examples of photometrically derived masses using SPS models can be found in Blanton & Roweis 2007; Drory et al. 2004.

Spectroscopy can also provide constraints on stellar mass, that in principle could be more detailed. For the SDSS Legacy Survey, which contains $\sim 10^6$ spectra of the centers of galaxies through 3 arcsec diameter fibers, Kauffmann et al. (2003) have performed an influential analysis using a combination of two spectral indicators (Section 2.2). These two indicators are the Hδ_A absorption index (representing the Balmer transition from $n = 2$ to $n = 6$ levels) and the D_n4000 index (which is representative of the 4000 Åbreak found in the spectra of galaxies). The use of this pair of indicators helps partially breaks the age-metallicity degeneracy (Worthey 1994). Kauffmann et al. (2003) use this model to constrain the M/L ratios of galaxies. They did so by using a suite of observed spectra from SDSS and a suite of SPS models, including ones with randomly distributed bursts of star formation, to fit for the spectra. They obtained 95% confidence limits on stellar masses of 0.2 and 0.3 dex. These results comprise the most commonly used catalog of physical parameters from the SDSS Legacy Survey, the MPA-JHU SFR and M_* catalog, upon which hundreds of subsequent investigations rely.

Surprisingly, the uncertainties in spectroscopically based stellar masses obtained by fitting observed optical spectra (Chen et al., 2012; Kauffmann et al., 2003) are not quoted to be significantly better precision than the color-based stellar masses, except for galaxies with

unusual SFH's Gallazzi et al. (2005). However, spectroscopically derived masses are more robust to systematic effects such as dust attenuation than photometric masses (i.e. stellar masses obtained by fitting broadband photometry).

An important practical point is that photometric measurements can generally measure the galaxy "as a whole" whereas in practice spectroscopic measurements are usually only of part of a galaxy. For example, in the case of Kauffmann et al. (2003), they determine M/L for the center of the galaxy and then apply that ratio based on the light of the galaxy as a whole. I investigate the effects of aperture correction in the MPA-JHU catalog using spatially resolved spectra over much broader region than 3 arcsec in Chapter 2.

Like the stellar mass, SFR measurements can be derived from photometric or spectroscopic measurements of the galaxy SED. As described above, there are scaling relations based on single measurements of UV or emission line flux which hold on average, but for individual galaxies are affected by the star formation history and dust models. In general, SED-based SFR's, when a fixed IMF is assumed, are consistent within a factor of two level (Conroy, 2013).

Later in this thesis, I will be relying on two representative estimates of SFR which rely on the interpretation of SEDs. The first, due to Salim et al. (2007a), used broadband photometry of SDSS galaxies and UV photometry from GALEX, interpreted using SPS models with a range of exponentially declining and bursty SFH's, metallicities and dust attenuation. They prescribed a specific, commonly used recipe for accounting for dust when using UV photometry, which shares much in common with a method usually used at high redshifts, known as the IRX-β method (see Overzier et al. 2011 and references therein). The second, due to da Cunha et al. (2008) and implemented in the software MAGPHYS, uses

UV, optical, and IR photometry to fit a self-consistent model to all of the data. The main difference is that MAGPHYS utilizes the IR data to constrain the dust reprocessing. I investigate in Chapter 1 the differences between these methods, using galaxy environments to assess whether using IR information yields correct additional information about the SFR.

In the SED modeling, the assumed SFH shape (i.e. star formation as a function of time) does matter. For instance, typically in the modeling of early-type galaxies, the SFHs are represented as an exponential decay function whose half-life is a parameter that is constrained by the SED fitting method used. The choice of priors on the SFH libraries can thus create systematic uncertainties in SFR estimation. The priors on dust modeling and the age-metallicity degeneracy inherent in SEDs can cause further challenges and thus, in the absence of high quality data, SFR estimations from SED fitting cannot be relied upon without a sufficient understanding the nature and extent of these biases.

For completeness, we note here that the MPA-JHU catalog contains SFR estimates based on SDSS spectroscopy. The catalog utilizes the method of Brinchmann et al. (2004), which fits to the emission lines a suite of optical emission lines with model parameters including metallicity, dust attenuation, ionization parameter, etc. It then applies an aperture correction based on the u-band flux in the images to account for the limited fiber radius, assuming the Hα to u-band flux ratio is constant. This last assumption is questionable. Nevertheless, comparisons of photometric SFRs to the MPA-JHU SFRs show that in general the two SFRs are in good agreement (e.g. Salim et al. 2007a). or using non-parametric SFH's.

The estimations of SFR and M_* of galaxies rely heavily of the availability and quality of data. Over the last decade, these have improved significantly, thanks to the high quality multi-band photometry as well as spectroscopy, including spatially resolved spectra, that

have been collected by various ground-based and space-based observatories. I review the significant observational surveys related to these observatories along with the major results gleaned from them in the following section.

0.4 Star Formation in the Local Universe

0.4.1 The Age of Digital Survey Astronomy

Redshift surveys in astronomy have their origins in the early 20th century when astronomers were interested in investigating Hubble's Law and the large scale structure of the Universe (Hubble & Humason 1931). The Center for Astrophysics (CfA) redshift survey (1977) was the first large systematic attempt at mapping a substantial contiguous volume of the sky and was later extended to the CfA2 survey which successfully obtained the spectra of over 15,000 galaxies in the 1990s (Huchra et al. 1995). With the advent of fiber-optic and multi-slit spectrographs allowing for simultaneous observations of hundreds of galaxies, larger redshift surveys such as the Las Campanas Redshift Survey (LCRS; Shectman et al. 1996) the Two-degree Field Galaxy Redshift Survey (2dFGRS; Colless et al. 2001) , the Sloan Digital Sky Survey (SDSS; Blanton et al. 2017; Eisenstein et al. 2011; ?), the Galaxy and Mass Assembly (GAMA) Survey, and others, have enabled astronomers to be able to study the physical properties of galaxies in a statistically rigorous manner.

The choice of survey (or sample of a survey) to study depends on the particular question in galaxy evolution that is being investigated. Thus, understanding the redshift limits of the survey (the so-called depth of a survey) or subsample that is being used to construct a volume-limited dataset is a crucial step in this process. In this thesis, we only concern ourselves with the local Universe out to redshifts of $z < 0.15$ as the goal is to understand the

limitations of some of the most commonly used SFR and M_* indicators. The angular coverage of a survey is also of importance, especially if environment measures play a significant role in the analysis. Keeping these in mind, the surveys I have worked with are derived from the SDSS Legacy sample.

SDSS is the largest spectroscopic and imaging survey of galaxies thus far. It has been carried out using a wide field 2.5-m optical telescope at the Apache Point Observatory (Gunn et al., 2006) in New Mexico, United States (Strauss et al., 2002; ?). SDSS imaging covers 14,555 square degrees on the sky (a little over 35%). It provides a uniform, well-calibrated map in *u, g, r, i* and *z* bands.

The spectroscopic SDSS Legacy Survey operated for eight years and covered 8,000 square degress on the sky, to a median redshift of $z = 0.1$ for the main galaxy sample and and out to $z = 6$–7 for the distant quasars. It used a multi-fiber spectrograph (Smee et al., 2013) to obtain the optical spectra of targeted galaxies. The spectra are taken using 3 arcsec diameter fibers and have a wavelength range of 3800–9200 Å. Some of the major results in galaxy formation and evolution have been possible because of the SDSS spectroscopic survey (see Section 0.4.2).

A major limitation of single-fiber spectroscopic surveys is that only a sub-region of the galaxy defined by the size of the fiber is sampled, which makes it more difficult to infer the galaxy's internal structure and dynamics or its global spectrum. To redress this problem, a number of integral field spectroscopic instruments have been built; they do not observe as many galaxies as the single-fiber surveys, but they observe them in greater detail. These instruments include Sydney-AAO Multi-object Integral-field spectrograph (SAMI; Bryant et al. 2015), Mapping Nearby Galaxies at APO (MaNGA; Bundy et al. 2014), and the MUSE

spectrograph. SAMI and MaNGA are being used to undertake large homogeneous samples of galaxies in the local Universe. MaNGA is the largest such survey of this nature so far, and aims to observe 10,000 galaxies by 2020 across a wide dynamic range in M_*, environment, and SFR with uniform radial coverage. I use this sample of galaxies to analyze the robustness of the aperture corrections made by Kauffmann et al. (2004) by looking at the galaxies through multiple apertures and comparing the observed M/L ratios obtained thus in Chapter 2.

In my analysis, I use the NASA-Sloan Atlas (NSA), a catalog of images and parameters of local galaxies up to redshifts of $z = 0.055$ that is derived from SDSS imaging, with additional UV broadband photometry from the space-based Galaxy Evolution Explorer (GALEX). The NSA is built from a reanalysis (Blanton et al., 2011) of the SDSS Legacy photometry, with improved object detection and deblending, making it better tuned for large, bright galaxies than the typical SDSS processing. The MaNGA target list is drawn from the NSA. This makes the NSA an ideal candidate to study the physical properties of galaxies in the Local Universe and I use the NSA to compare two star formation indicators in the context of dust in Chapter 1.

0.4.2 Studying Star Formation in the Local Universe

Large observational surveys such as the SDSS have, over the last two decades, enabled us to make accurate measurements of tracers of important physical properties of hundreds of thousands of galaxies across a wide redshift range. These measurements have in turn informed some of the most important results in reconstructing the cosmic star formation history of the Universe and understanding the process of galaxy formation and evolution.

In this section, I will discuss some of the most important trends observed, their significance in galaxy evolution and finally, the need for robust SFR and M_* measurements, thus motivating the work in this thesis.

Strateva et al. (2001) observed, using SDSS imaging, the bimodality of galaxies, i.e., that there were two distinct populations of galaxies, a blue, star-forming population and a population of red, passive galaxies that have little or no star formation. As Blanton & Moustakas (2009a) review, this bimodality is related to galaxy morphological types; blue galaxies are spiral galaxies and red galaxies are early type spiral, lenticular, or elliptical galaxies.

The relationship between galaxies and their dark matter halo hosts, particularly in the context of galaxy clusters, has been investigated by looking at galaxy clustering measurements. The passive non-star-forming large ellipticals preferentially exist in the center of these haloes (Zheng et al., 2005). Thus, for a sufficiently large local sample of galaxies, the star forming galaxies preferentially exist in lower environments and the passive "quenched" population preferentially exist in clusters. These trends again reflect the long-known segregation of morpghological types (Dressler 1980).

Galaxies without star formation must have been galaxies with star formation at some point in their past. The intermediate population of galaxies, the so-called "green valley" (Wyder et al., 2007) or more aptly, the transitioning galaxies (i.e., the galaxies that are in the process of transitioning from star-forming to quenched), is thus a population of wide interest. Observationally, these are harder to identify without understanding the role of dust in obscuring galactic starlight, and thus their physical properties are not entirely apparent.

It has also been found that for star forming galaxies between redshifts of $0 < z < 4$, there is a tight relation between galaxy star formation rates and their stellar masses, known

as the star forming main sequence (SFMS) ([Brinchmann et al., 2004](#); [Noeske et al., 2007](#); [Schreiber et al., 2015](#)). This is usually observed as a power law relationship with SFR $\propto M^\alpha$, with an intrinsic scatter of 0.2-0.3 dex for moderate to relatively low mass galaxies. Recent investigations into the SFMS suggest that the value of α is between 0.6-1.2 ([Speagle et al., 2014](#)). Over cosmic time, the SFMS moves to lower star formation rates, which is the primary driver of the change in the cosmic star formation rate density ([Madau & Dickinson 2014](#)). At the same time, some galaxies leave the SFMS completely and become quiescent ([Hahn et al. 2015](#); [Moustakas et al. 2013a](#)).

The question of how galaxies move off the SFMS to become quiescent or quenched, i.e. how galaxies turn off the process of star formation, is fundamental to the study of galaxy evolution, as we have seen in Section 0.2.3. In broad terms, two different process have been proposed for this: internal processes that quench star formation such as AGN or supernova feedback ([Peng et al., 2010](#)) and external processes such as environmental effects which strip the galaxy of its gas content ([Geha et al., 2012](#); [Peng et al., 2012](#)). As ? point out, because galaxy scaling relations remain constant with environment even as the relation numbers of different galaxy types change, it is likely that internal processes are primarily driving the evolution of galaxies — otherwise, the formation process of, say, an elliptical galaxy in the field would be different than the formation process of an elliptical in a cluster, even though the two populations of galaxies follow the same relationships.

Galaxy formation theorists seek to address these questions by employing semi-analytical models or hydrodynamic simulations that reproduce the diversity of observations we see ([Somerville & Davé 2015](#)). These theories are beginning to make detailed predictions that match observational results, but they rely on subgrid physics that require calibration. For

example, it is now standard for theoretical models to calibrate their unknown subgrid parameters to the stellar mass function and SFMS at $z \sim 0$. Then variation of galaxy properties with environment or redshift becomes a prediction of the model. In addition, theorists often interpret agreement with observations as validation for the characteristics assumed of the subgrid model.

The precision with which the theories can match the stellar mass function and SFMS is increasing, and the predictive and interpretative power of the simulations therefore are increasing. For this reason, it is highly important to test the accuracy of the observational calibrations for the models. If the observational results to which the simulations are calibrated are in error in a systematic, that error propagates into the further predictions and the further interpretation of the simulations.

This thesis explores two areas of importance in testing the robustness of the observations. First, it considers estimates of SFR and the relative importance of accounting for dust extinction and reemission. Specifically, I test in a new empirical way whether infrared-based SFR estimates such as da Cunha et al. (2008) yield more accurate star formation indicators than ultraviolet indicators. Since the ultraviolet indicators are the most accessible ones for high redshift observations, this topic is related to how reliably we can measure evolution of the SFMS.

Second, it considers aperture effects on estimates of stellar mass. specifically I use new integral field spectroscopy observations to test fiber aperture effects in the methods of Kauffmann et al. (2003). These methods have been adopted by hundreds of investigations based on the SDSS Legacy Survey and are highly influential.

0.4.3 THIS THESIS: EMPIRICAL STAR FORMATION ESTIMATES

In this thesis, I focus on evaluating the possible systematic effects in two ubiquitously used measurements of star formation in the field of galaxy evolution, the UV star formation rate and the stellar masses estimated in the largest catalog of measurements of physical properties of galaxies, the MPA-JHU Catalog.

In Chapter 1, I evaluate the robustness of UV star formation rates in tracing star formation activity, especially in dust-obscured galaxies which might appear to be redder than they are in optical color. The steps towards doing this involve choosing an appropriate nearby galaxy sample (Section 1.2), estimating two different star formation rates - one relying purely on ultraviolet photometry and another, using UV-to-IR photometry with an SED fitting method that uses a physically motivated model for dust (Section 1.3), using galaxy environments to be able to identify the dust-obscured optical green valley galaxies (Section 1.4) and finally, evaluating which star formation rate is able to trace star formation activity in dust-reddened star formers better (Section 1.5).

In Chapter 2, I examine the possible systematic effects in the stellar mass estimation method used in the MPA-JHU catalog due to aperture bias. To this end, I use spatially resolved spectroscopic data from the largest IFU-based survey designed thusfar (Section 2.1) and employ variable apertures to obtain the spectra that would fall within 3" apertures at various redshifts (Section 2.3.3)and evaluate the two key spectral indicators (Section 2.2) that are used to constrain the mass-to-light ratios of the galaxies in the catalog, thus reproducing the Kauffmann et al. (2003) method. I then examine how offset the mass-to-light ratios are from what they would be with a full aperture (i.e., if the "entire" galaxy were to fall within the aperture) and the implication of the trends in these offsets (Section 2.5).

1

UV to IR Star Formation Indicators and Environments

Determining the formation history of galaxies is one of the most important tasks in astronomy. The average star formation rates of galaxies have reduced with cosmic time (as reviewed by Madau & Dickinson 2014) and star-forming galaxies "transition" to red and quiescent ones over that time (*e.g.* Ilbert et al., 2013; Moustakas et al., 2013b; Muzzin et al., 2013; Peng et al., 2010; Tomczak et al., 2014, among others). Many mechanisms have been proposed to explain the observed patterns of galaxy evolution but there are many unresolved questions regarding them. These mechanisms are known to have a some correlation with the environment, due to the fact that galaxy type depends on environment in the present day (Blanton & Moustakas, 2009a; Dressler, 1980).

Star formation rate estimates are an important tool in the observational study of this problem (Kennicutt & Evans, 2012). The light emitted from galaxies can reveal recent star formation through the ultraviolet light of massive stars, recombination line emission in the ionized gas around those stars, in infrared light from dust in the galaxies absorbing the ultraviolet starlight, and from radio synchrotron emission from the ionized gas. Ultraviolet, optical, and infrared images and spectra are available for numerous low redshift galaxies, from the Sloan Digital Sky Survey (SDSS; York et al. (2000)), the Wide-field Infrared Survey Explorer (WISE; Wright et al. (2010)), and the Galaxy Evolution Explorer (GALEX; Martin et al. (2005)).

In this chapter we compare two specific ways to estimate star formation rates from imaging photometry. We concentrate on imaging because it usually provides the most complete census of the galaxy; spectroscopy is often of only part of the galaxy, usually the center. We

are interested specifically in comparing ultraviolet-based star formation indicators with indicators that account for the infrared light. The main difference between these types of indicators is how they account for dust absorption. The former ostensibly are corrected for dust absorption, but we generally expect that the latter should be more reliable and complete. However, detectable infrared light is not always available.

The presence of dust is an important complication in any analysis of galaxy light. Dust absorbs preferentially in the UV/optical region of the galaxy spectrum and both extincts and reddens the photometric data. The extinction in the visual bandpasses in star forming galaxies is highly variable but is commonly of order 50%. This energy is re-emitted in the mid- to far-IR by poly-cyclic aromatic hydrocarbon molecules as well as warm and cold dust grains. Recent studies (Burgarella et al. 2013) find that in the nearby universe, almost 70% of the FUV luminosity is obscured by dust on an average. Although UV estimates of star formation do attempt to account for dust attenuation (Salim et al. (2007b)), the extensive reliance on UV SFR in the literature (*e.g.* Karim et al., 2011; Lee et al., 2009; Moustakas et al., 2013b; Peng et al., 2010; Wyder et al., 2007, among others) makes it important to understand how well the dust corrections for UV SFR estimates work relative to other methods of estimating SFR.

Here, we examine a sample of galaxies whose UV-IR photometry is available and estimate the star formation rate in two independent ways. First we exploit the fact that we have UV to IR photometry and perform SED fitting using MAGPHYS (da Cunha et al., 2008), which accounts for dust by using a simple method of energy balance to obtain the specific star formation rates (SSFRs). The other method involves using purely UV photometry to estimate both star formation rate and dust attenuation using the prescription given by

Salim et al. (2007b). We also estimate the environments of our population. We ask the following questions of this sample. How do these different star formation estimators disagree with each other? How does each estimate correlate with environment? Does one trace environment more closely? Under the assumption that the environment primarily correlates with the SSFR rather than dust obscuration's effect on the observables, studying this correlation will yield insights into the relative accuracy of the methods.

1.2   Constructing a local sample spanning Ultraviolet to Infrared Imaging

The sample on which we perform our measurements is based on the NASA-Sloan Atlas, a nearby galaxy sample which includes optical and ultraviolet imaging from SDSS and GALEX. We use NSA version v0_1_2, whose redshift range extends up to $z = 0.055$ and includes SDSS (Data Release 9) and GALEX imaging for galaxies. The total number of objects in this NSA catalog is $\sim$150, 000. We define two samples from the NSA, one that we use to define environment (Environment Determining Population or EDP, hereafter) and one for which we determine star formation rates (Star Formation Rate Population or SFRP hereafter). We note that the SFRP is a subsample of the EDP. To get our EDP, we impose a volume-limited cut on this sample by retaining only galaxies with $-24.5 < M_r < -18.5$, which leaves us with 95, 638 galaxies.

The star formation rate determinations we use here require both UV data and IR data. About 80% of our galaxies have UV data from GALEX analyzed in the NSA. To obtain infrared imaging for the data we use the Wide-Field Infrared Survey Explorer (WISE) data and match the objects from the NSA with the ALLWISE Source Catalog to get the four-band infrared fluxes for each galaxy. About 99% of galaxies in this sample have WISE data.
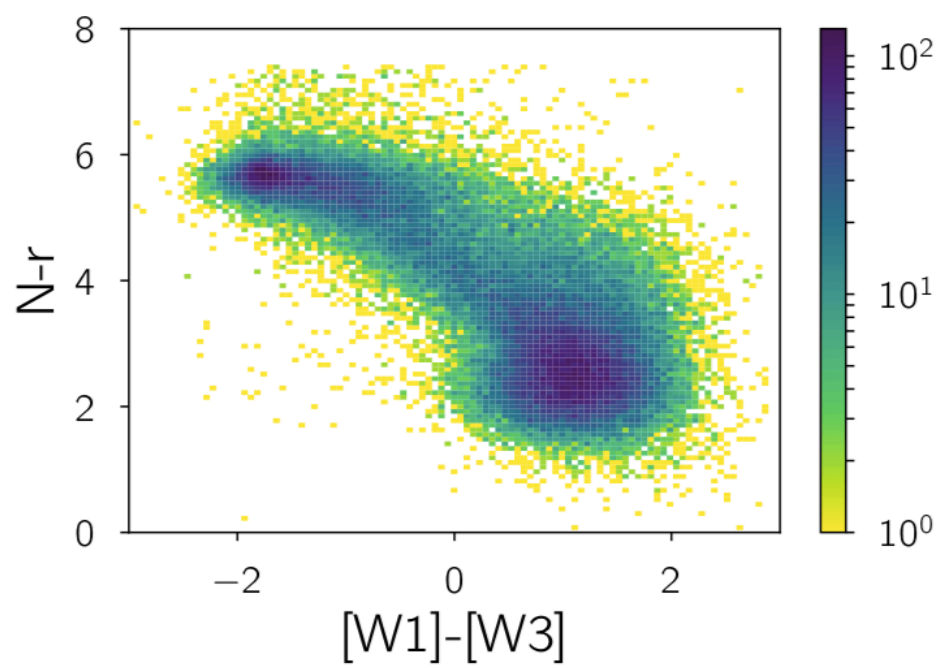
Figure 1.1: The local sample distribution across optical and IR colors

We intend to study the evolution of these galaxies through the optical-IR color space, and therefore remove all galaxies with missing/faulty photometry in GALEX, SDSS, or WISE. This process includes limiting the color range of objects in the optical ($7.5 > N - r >= 0$) and infrared ($3.0 > [W_1] - [W_3] >= -3.0$) colors (top left corner of Fig. 1). In addition, we remove some objects near the edges of the sample, which do not have reliable environment determinations (see Section 1.4.2). Our SFRP ultimately consists of 61, 046 objects with absolute magnitudes in the UV (F and N bands), optical (u, g, r, i and z bands) and infrared (W_1, W_2, W_3 and W_4 bands). While the k-corrected magnitudes are available for the optical and UV bands, we had to reasonably account for them for the WISE bands. To this end, the k-corrections were obtained for the WISE bands iteratively by using MAGPHYS to re-calculate them and were found to converge after the second iteration.

1.3 Estimating the Specific Star Formation Rates

We compare two approaches to calculating specific star formation rates (SSFRs). The first uses UV, optical, and IR data. The second uses only the UV data.

1.3.1 SED Fitting - MAGPHYS

We develop here a method to quickly estimate SSFRs based on UV-optical and infrared colors. We begin by sorting galaxies into bins of the ($N-r$) - ($[W_1]-[W_3]$) color space (25×25 bins, where the optical and IR bin sizes are 0.29 and 0.24 in magnitudes respectively). Within each bin, we normalize the fluxes of each galaxy relative to a constant flux in the r-band, and then take the mean normalized flux in each band over all galaxies in the bin. This procedure yields a "template" SED for each bin in the color-color space.

We then use Multi-wavelength Analysis of Galaxy Physical Properties (da Cunha et al. (2008)) software to infer the SSFR for each template SED. MAGPHYS is a physical model-based method to interpret the mid- and far-infrared spectral energy distributions of galaxies, self-consistently modeling the emission at ultraviolet, optical, and near-infrared wavelengths. For every input galaxy with a set of observed fluxes in different bands, MAGPHYS generates an optical and infrared library at that redshift and then samples all template spectra whose fluxes obey a simple principle of energy balance: that the amount of energy absorbed by dust in the UV/Optical matches the amount of infrared emission that is accounted for purely by dust. Once the templates have been sub-sampled thus, MAGPHYS uses chi-squared fitting to see which combination best reproduces the observed fluxes along with the likelihood for the distributions. The results for the SSFRs thus obtained for each template are shown in the lower left panel of Fig 1.2 along with the number distribution of the galaxies across the chosen bins. Note that bins with < 5 galaxies were omitted as those regions of the color-color space are obviously under-sampled.

The resulting distribution of the MAGPHYS-based SSFRs across the color-color space looks as we would expect it to for the most part. In UV-optical colors, blue galaxies have high SSFRs, and red galaxies have low SSFRs. However, there is also a dependence of SSFR on IR color; most notably, in the UV-optical green valley, the redder galaxies in the IR have higher SSFRs. These galaxies are likely to be dust-extincted in the UV, with the reemission by dust reddening the IR colors. In what follows, we will use the UV-optical and IR colors of individual galaxies, and the dependence of the SSFR on these colors shown in the lower left panel of Fig 1.2, to assign an SSFR to each individual galaxy.

1.3.2 UV Star Formation Rates

We also explore a simple method of determining star formation rates developed by Salim et al. (2007b) that depends only on the UV fluxes of each galaxy. It assigns a star formation rate that is proportional to the UV luminosity (specifically the FUV band if we are looking at GALEX). Dust attenuation is also accounted for in this method by looking at the ratio of luminosities in the FUV and NUV bands.

According to this prescription (Salim et al., 2007b), the star formation rate is given by:

$$SFR = 1.08 \times 10^{-28} L^{\circ}_{FUV},$$

where L°_{FUV} is the rest-frame FUV luminosity. This method accounts for dust attenuation of the FUV light as well by estimating an attenuation factor Av as follows.

If $N - r \geq 4.0$, i.e. for the red sequence galaxies,

$$Av = \begin{cases} 3.32(F - N) + 0.22, & \text{if}(F - N) < 0.95 \\ \\ 3.37, & \text{if}(F - N) \geq 0.95. \end{cases}$$

If $N - r < 4.0$, i.e. for the blue sequence galaxies,

$$Av = \begin{cases} 2.99(F - N) + 0.27, & \text{if}(F - N) < 0.90 \\ \\ 2.96, & \text{if}(F - N) \geq 0.90. \end{cases}$$

This method uses the UV slope to estimate the dust attenuation. The physical idea is that when the UV light is dominated by massive young stars, these are hot enough that we

are observing their Rayleigh-Jeans tail spectra, and this slope is basically constant with age of the population. Thus the observed UV color reveals the dust reddening.

The lower right panel of Fig. 1.2 shows the mean $SSFR_{UV}$ as a function of color. Compared to the lower left panel, the $SSFR_{UV}$'s have a nearly monotonic relationship with UV-optical color whereas, as discussed above, the $SSFR_{MAGPHYS}$'s do not. Assuming the $SSFR_{MAGPHYS}$'s are closer to correct, the UV-optical green valley contains a population of galaxies that are not truly transitioning but instead are reddened by the presence of dust. Furthermore, the nominally dust-corrected UV star formation rates do not successfully identify these galaxies.

1.4 ENVIRONMENTS

We identified above a population of galaxies isolated in color space, which appeared to have dust-extincted star formation, such that the $SSFR_{UV}$ estimate was much less than the $SSFR_{MAGPHYS}$. In order to confirm whether MAGPHYS is capturing an inherent property in this population of galaxies, we examine an independent physical property, namely the environments of our sample.

1.4.1 MEASURES OF ENVIRONMENT

The environment of a galaxy can be defined in many ways, such as fixed aperture counts, distance to the nth nearest neighbor, Voronoi volumes, etc (Cooper et al., 2005). Here we use counts in a projected fixed aperture of radius 0.5 Mpc as our environment measure. Around every galaxy we construct a projected cylinder with a radius (in the transverse direction) of $r_t = 0.5$ Mpc and a line of sight velocity window of $v_{los} = \pm 1000 km/s$. For each
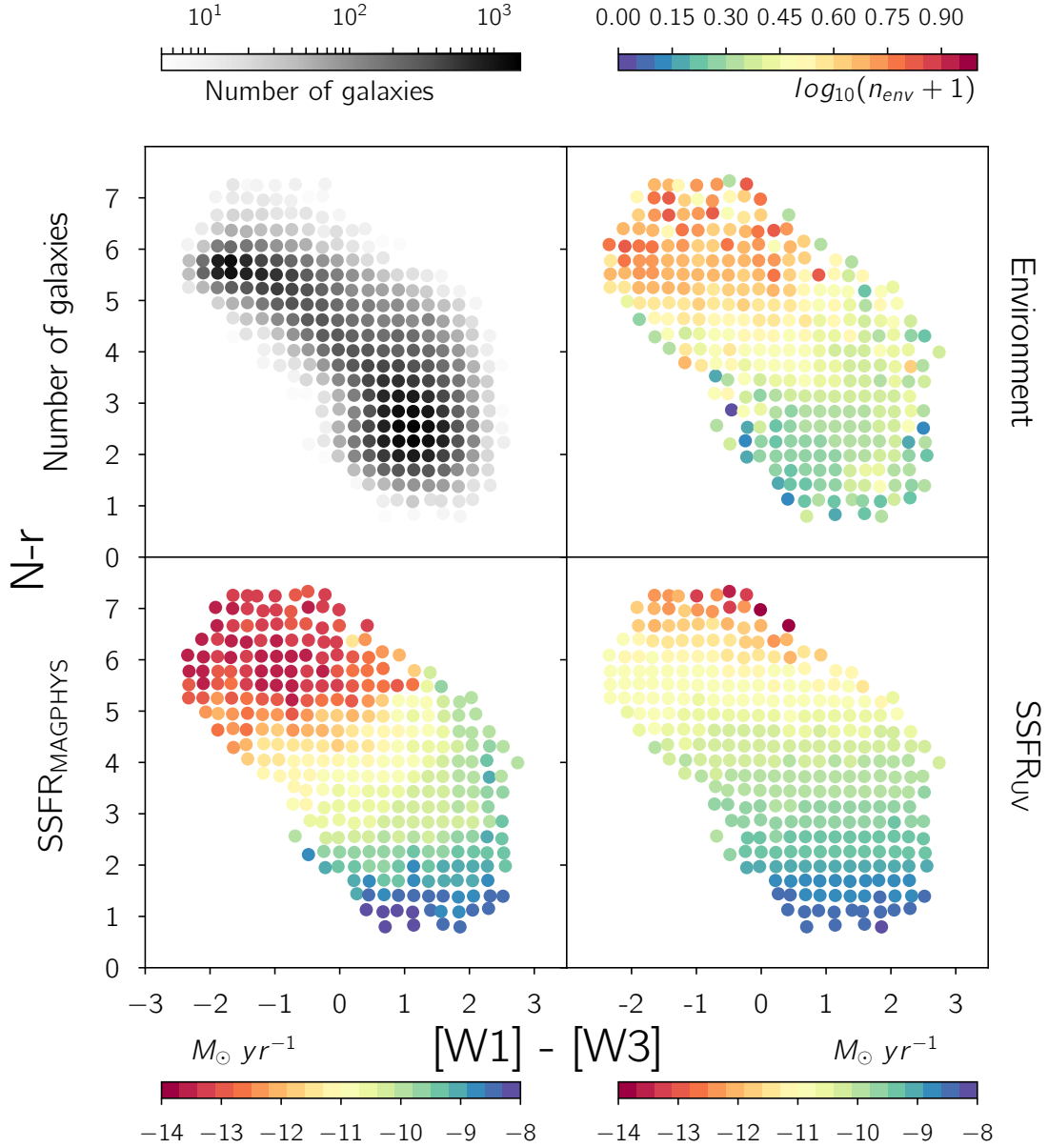
Figure 1.2: The SSFR measurements and environment shown the color-color space. Each point in the plot is shown at the mean colors in each of the bins we use. The grey value or color of the points in each panel show the mean value in each bin for the quantity described by the corresponding color bar. *Top left:* Logarithmic number density in each of the bins; all bins with less than 5 galaxies were discarded in this and the other panels. *Top right:* Environment; in each bin, the average number of nearest neighbors is calculated in a projected cylinder ($r_t = 0.5 Mpc$ and $v_{los} = \pm 1000 km/s$). *Bottom left:* the Specific Star Formation Rates obtained from MAGPHYS. *Bottom right:* UV Specific Star Formation Rates estimated by using the method described in Salim et al. (2007a).

galaxy for which we have star formation measurements, we count its number of neighbors (n_{env}) in this cylinder(Fig. 1.2) in the Environment Defining Population.

1.4.2   Edge Effects

We must also account for the survey edges. For galaxies at the edge, part of the fixed aperture used to estimate the environments might lie outside the survey coverage. It is important to identify these galaxies and either discard them or assign an appropriate weight to n_{env} in order to account for the missing area.

To identify the edges, we use (Swanson et. al.'s) `Mangle`, a suite of free open-source software designed to deal with complex angular masks in an efficient and accurate manner. First, the NYU-VAGC `Mangle`-format mask was used to obtain the angular mask for the NASA Sloan Atlas by using the *polyid* routine from `Mangle`. Then, the *ransack* routine was used to populate the mask with a random sample of $N = 10,000,000$ galaxies. For each galaxy, we compute the angular separation ϑ_i that corresponds to our $0.5 Mpc$ aperture at the redshift of that galaxy. We then count the number of galaxies n_i that lie within this angular separation and compare the value obtained to the expected value:

$$\langle n \rangle_i = \frac{N}{A_{EDP}} \times \pi \vartheta_i^2 \times f_{thresh}$$

A_{EDP} is the total area of the mask and f_{thresh} is the fractional threshold for the edge effect cut-off. In our case, we chose $f_{thresh} = 0.8$. Wherever $n_i < \langle n \rangle_i$, we consider the galaxy to be near an edge and discard it from our sample.

1.4.3   Environments in Color-Color Space

The mean environment, quantified by $(\langle n_{\mathrm{env}} \rangle + 1)$ in each bin are shown in the upper right panel of Fig. 1.2 as a function of optical and infrared colors. As we expect from many previous studies (Blanton & Moustakas 2009b) the star-forming bluer galaxies tend to exist in less dense environments on average and the red-and-dead population tends to exist in more dense environments. In the UV-optical green valley region $(3 < N - r < 5)$ there is some indication that the environment declines with $[W1] - [W3]$ color at fixed UV-optical color. However, the mean environments in this plot cannot easily be interpreted, because the mean stellar mass in each bin is different, so some of the variation is driven by the dependence of environment on stellar mass.

1.5   The Environments of the Outliers

Fig. 1.3 shows the relationship between the two SSFR measurements, with points colored according to the mean environment, for each bin in color-color space from Fig. 1.2. There is a set of bins in the range $-10.5 < \mathrm{SSFR}_{\mathrm{MAGPHYS}} < -9.5$ that have lower $\mathrm{SSFR}_{\mathrm{UV}}$ values than the general trend, and have environments similar to the other galaxy bins in the same MAGPHYS range. Hereafter we shall refer to this population as the "Outliers," to distinguish them from the general trend line in Fig. 1.3.

We identify these outliers more specifically in Fig. 1.4(a), as being in the lower right square. The galaxy bins with the same $\mathrm{SSFR}_{\mathrm{MAGPHYS}}$ values (above the square) are identified as the "MAGPHYS Box" and the bins with the same $\mathrm{SSFR}_{\mathrm{UV}}$ values (left of the square) are identified as "UV BOX" in Fig. 1.4(a).
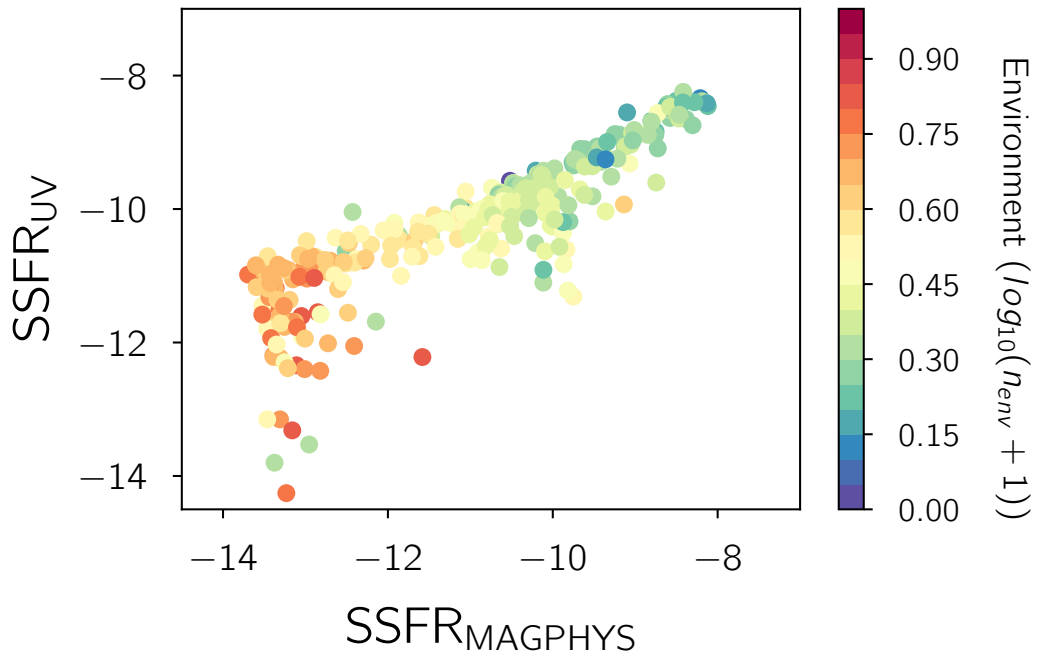
Figure 1.3: The two star formation rate estimates (from Fig.1.2) plotted against each other as a function of the environment; We notice two distinct set of outliers that seem to have lower UV SSFR's but similar environments to the galaxy bins with the same MAGPHYS SSFR's.
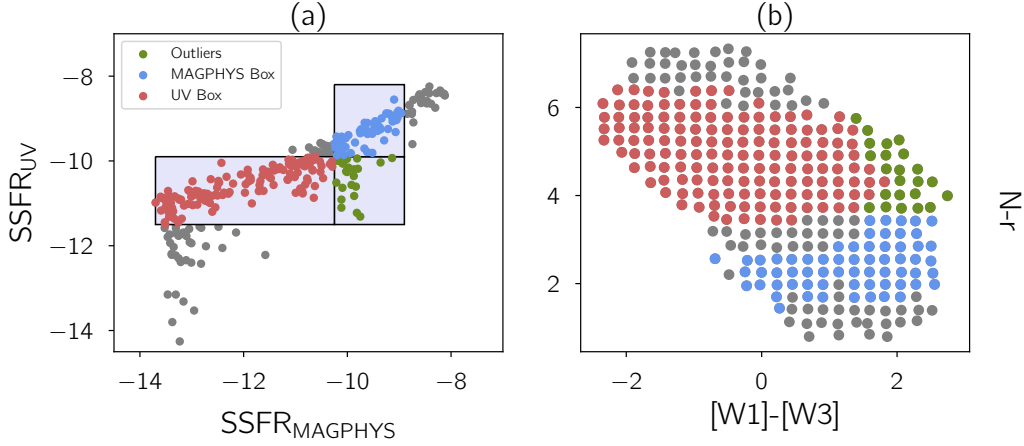
Figure 1.4: The outliers shown as a function of the Star Formation Rates as well as Optical and IR colors

1.5.1 GREEN-VALLEY INTERLOPERS

When we return to the color-color space (Fig. 1.4(*b*)) and show where the bins in each box lie, we see the trends we would expect. The Outliers lie in a similar UV-optical color range as the UV box but have higher IR color. The MAGPHYS Box occupies the bluer side in the optical color range while spanning almost the entire IR color range. The UV Box occupies the redder side in the optical color range while having lower IR color values. The Outlier bins are the same bins we previously identified as the galaxies in the UV-optical "green valley" that are there due to dust reddening.

To verify this, we unwrap the bins and look at the Probability Density Function of the Environments of the galaxies in these three regions in the mass range $9.5 < M_* < 10.7$ and examine the distribution of environments in these three regions, the result of which is plotted in Fig. 1.5.

1.5.2 Jackknife Errors

To calculate uncertainty in the estimated probability density functions of the environments, $P_{i,\text{bin}}$'s $: i = 1, 2, 3$ for each of the populations, we use the standard jackknife technique. Jackknife re-sampling gives us an internal error estimate that tests how representative a measurement/trend is of the data it is estimated with. We divide our entire sample into 20 subsamples with nearly equal co-moving volumes and estimate the same probability density functions(P_i^j's) for the whole sample while leaving out one subsample each time. We can then estimate our uncertainty for each bin in the PDF's thus:

$$\sigma_{i,\text{bin}} = \sqrt{\frac{N}{N-1} \sum_{j=1}^{j=N} (P_i^j - P_{i,bin})^2}$$

The errors estimated in this manner account for Poisson shot noise and also the sample variance, the extra error associated with the fact that the density field varies across the survey. Although precision studies of large scale structure have found that latter effect is not perfectly accounted for with standard jackknife techniques, they are precise enough for our purposes here. The jackknife errors are shown in Fig. 4 and confirm our hypothesis: that the Outliers are a little different than the MAGPHYS Box but still, very different from the UV Box.

1.6 Summary and Conclusion

From the analysis presented above, we can conclude the following:

- From Fig 1, we see that $\text{SSFR}_{\text{MAGPHYS}}$ identifies a region in the color-color space as dust-obscured star forming galaxies and correlates better with the environments of
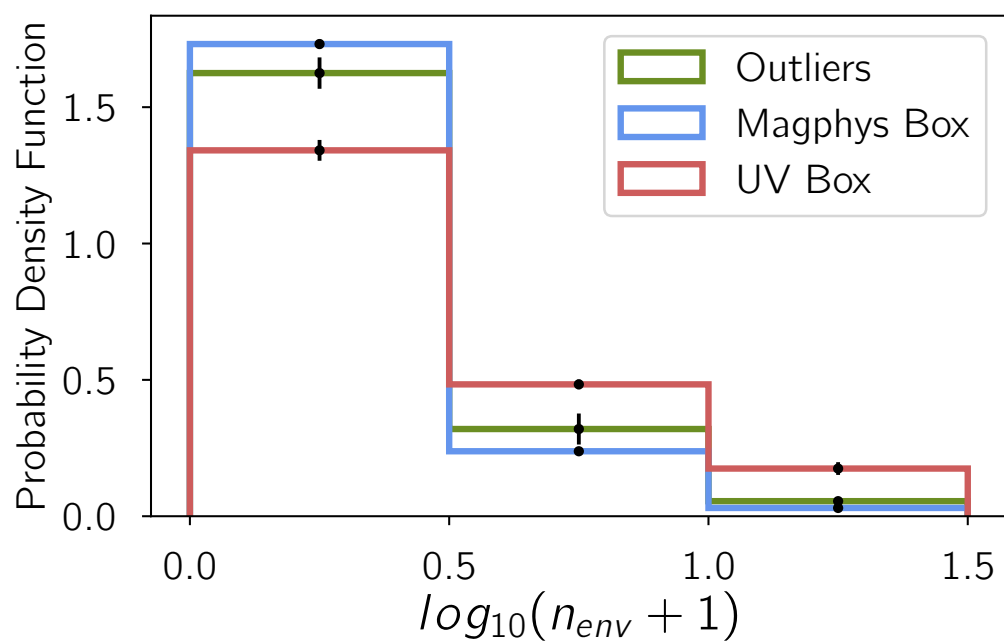
Figure 1.5: Probability density functions of the Environments of the three populations described in Fig. 2

the galaxies.

- At the higher star formation end, we find that the dust-obscured star-formers as identified by MAGPHYS have environments comparable to the blue star-forming galaxies, confirming that this is indeed a physical effect we're seeing.

- Comparing the environment distribution of the Outliers relative to the galaxies with (a) the same $SSFR_{MAGPHYS}$'s as the Outliers and (b) the same $SSFR_{UV}$'s as the Outliers (Fig. 1.5), we find that the Outliers indeed have a similar environment distribution to the galaxies that have the same $SSFR_{MAGPHYS}$'s, i.e., they seem to favor lower environment densities mimicking the behavior of star-formers.

This points at a more significant trend in that the widely used UV star formation rates, in the optical green valley region of the color-color phase space, are not able to meaningfully distinguish between the galaxies with intermediate star formation rates from the dust obscured star-formers. Further, the inclusion of information in the infrared is crucial to be able to catch the dusty interlopers here. This surmise is backed by evidence from the galaxy environments for the dust-obscured star formers which resemble the a population of galaxies with the same IR-based star formation rates in the much more closely than the ones with the same UV-based star formation rates. Many high-redshift surveys rely significantly on UV based star formation rates and this could be a cause for concern in the regions where they fail and in particular, obtaining IR information would be critical in accurately estimating star formation activity in the presence of dust.

2

Aperture effects in Stellar Mass Estimates

In this chapter we investigate methods of constraining the star formation histories and stellar masses of galaxies where galaxy spectra are available. In particular, we look at the largest galaxy catalog of estimated stellar masses, star formation rates and gas metallicities, the MPA-JHU catalog (Brinchmann et al., 2004; Kauffmann et al., 2003; Tremonti et al., 2004), obtained from spectra from the Sloan Digital Sky Survey (SDSS) Legacy Survey. The MPA-JHU catalog has, over the last decade and a half, been one of the most influential and widely-used catalogs in the fields of galaxy formation and evolution; the original catalog paper of Kauffmann et al. (2003) has been cited over a thousand times. Here we test a fundamental assumption of the catalog, which is that spectroscopic measurements of the central region of the galaxy yield sufficient information to constrain star formation histories and stellar masses for the galaxy as a whole.

The importance of galaxy star formation histories has been discussed in Sections 0.2.3 and 0.4.2. Crucial to analyzing these histories are accurate inferences of star formation rates and stellar masses from observed data. In particular, the stellar mass function, which is used to calibrate the parameters in simulations that seek to reproduce the star formation histories of galaxy populations, relies on accurate observational calibrations of stellar mass. In this spirit, I examine one of the most widely used stellar mass estimation methods; this method from Kauffmann et al. (2003) involves two spectral indicators and uses an aperture correction to account for the limited spatial resolution coverage of SDSS spectra. I investigate the robustness of this method using spatially resolved spectra from the Mapping Nearby Galaxies at Apache Point Observatory survey (MaNGA; Bundy et al. 2014).

2.1.1 THE SDSS SPECTRA

As introduced in Section 0.4.1, SDSS has been conducting a coordinated imaging and spectroscopic survey since 2000 and is currently in its fourth phase of operation. The first two phases of the survey, SDSS and its extension SDSS-II, ran from 2000–2008 and took spectroscopy over approximately 8,000 square degrees of mostly the northern galactic sky ran between 2000-2008. It served as the primary database for the MPA-JHU catalog (Brinchmann et al. 2004; Kauffmann et al. 2003; Tremonti et al. 2004), whose final results were published in SDSS's Data Release 8 (DR8), which contains observed spectra of a little over 900,000 galaxies (Aihara et al., 2011).

The imaging and spectroscopic data were observed using a 2.5 m telescope at the Apache Point Observatory (APO) in Sunspot, New Mexico. The imaging data was obtained by using a wide-field mosaic CCD camera and the spectroscopic data, using twin multi-object fiber spectrographs (Smee et al., 2013), all of which are mounted at the Cassegrain focus of the telescope. The imaging survey, which is carried out in drift-scanning mode using a 5×6 array of 2048×2048 pixel detectors, obtains photometry in the u, g, r, i and z bands. This broadband photometric data, after reduction and calibration, serves as the pool of data from which spectroscopic target selection is then done. The spectroscopic fiber plug-plates are aluminum plates which have holes drilled into them at positions decided upon by the target selection and the optical fibers are plugged into into these holes. They have a circular field-of-view of radius 1.49 degrees and during SDSS-I and -II were outfitted with 640 fibers, allowing for simultaneous observation of 640 spectra (mostly galaxy spectra and some which are reserved for standard and blank sky observations for calibration) in a 3 degree diameter field of view over the course of a single exposure.

The fiber diameter of the optical fibers was chosen with a view to maximize the signal-to-noise (S/N) ratio for an extended source, keeping in mind the sky conditions at APO. The optimal choice that was decided upon corresponds to a fiber diameter of 180 μm or 3". The rest-frame wavelength range of the spectra at the median redshift is from 3500 Å to 8500 Å with a spectral resolution:

$$R = \frac{\lambda}{\Delta\lambda} \approx 2000.$$

The spectra are calibrated using observations of F stars in each 3 degree field.

SDSS imaging data and spectra have played a significant role in many discoveries in astronomy and cosmology over the last decade and a half. In addition to fundamental measurements of cosmological parameters and the study of distant quasars and stars in our own galaxy, the Main Sample of galaxies in SDSS-I and -II (?) has informed much of the new understanding of galaxy properties that we have today. This new understanding has included the quantification of the bimodal nature of galaxy properties cites, the relationship between galaxy properties and environment cites, and how galaxy properties relate to the masses and other properties of their host dark matter halos cites. Key to many of these works has been the use of new ways to estimate star formation histories, stellar masses, and chemistry of stars in galaxies, including those found in the MPA-JHU catalog. I discuss the catalog and the methods used to estimate these quantities in the following sections.

2.1.2 THE MPA-JHU CATALOG

The MPA-JHU catalog is the result of a collaborative effort between a group of researchers at the Max Planck Institute for Astrophysics and the John Hopkins University and was

first constructed for the first SDSS Data Release (DR1) of spectroscopic observations. The original dataset they used was 120,808 galaxies drawn from the SDSS DR1 for which the following properties were estimated: stellar masses and mass-to-light ratios, effective stellar attenuation by dust, indicators of recent major starbursts, current total and specific star-formation rates, gas-phase metallicities, AGN classifications based on the standard emission line ratio diagnostic diagrams and AGN luminosities. The methods of estimation of these properties can be found in Kauffmann et al. (2003) for the stellar masses, Brinchmann et al. (2004) for the star formation rates and Tremonti et al. (2004) for the gas phase metallicities.

The MPA-JHU catalog measurements are ubiquitous in galaxy evolution literature with many important results relying on the inferred SFR's, masses and metallicities from the catalog. A few examples of scientific results from which the significance of the catalog can be evinced would be: understanding the host galaxies of AGN's by Kewley (Kewley et al., 2006), the star formation-density relation and its reversal in distant universe by Elbaz et al. (2007), constraining the mass-metallicity relationship for star-forming galaxies (Kewley & Ellison, 2008), the mass dependence of radio-loud AGN's (Best et al., 2005), insights into quenching mechanisms (Peng et al., 2010) and large scale galactic conformity (Kauffmann et al., 2013), mapping the stellar mass function (D'Souza et al., 2015; Li & White, 2009), and many others.

The MPA-JHU catalog uses SDSS spectra to constrain the stellar masses and star formation histories in the catalog by looking at two key spectral indicators of starbursts and age of a galaxy: the Balmer $H\delta_A$ absorption line index and the D_n4000 break index. Because they are both measurements defined over a narrow range of wavelengths in the blue, that are similar to each other, and are independent of the absolute flux, they are designed to be

insensitive to dust extinction within the galaxy. The indices are discussed in detail in Sections 2.2.1 and 2.2.2. Using the distribution of the observed galaxies in the $H\delta_A - D_n4000$ plane and by employing Stellar Population Synthesis (SPS) models by Bruzual & Charlot (2003b) to model the evolution of galaxies in this plane, they are able to derive maximum likelihood estimates of the stellar mass of a galaxy (Kauffmann et al., 2003), the attenuation of optical light by dust and the fraction of stars in a galaxy formed in recent bursts.

The spectra are only of the center of the galaxy so do not on their own constrain the total stellar mass. What is actually inferred from each spectrum at a given point $H\delta_A - D_n4000$ phase space is the mass-to-light ratio in the z-band for models that are at that same point. Now, as we have just seen in Section 2.1.1, due to the nature of fiber spectroscopy, the angular area of coverage of a galaxy observed is limited to $3''$, which could correspond to different actual physical sizes depending on the redshift of the galaxy. Thus, Kauffmann et al. (2003) (and in a similar way for SFRs, Brinchmann et al. 2004) prescribe a method of aperture correction that relies on the assumption that the mass-to-light (M/L) ratio of the central part of a galaxy is representative of the entire galaxy. Thus the fiber M/L ratios are obtained in the z-band are multiplied by the luminosity of the galaxy in the z-band, that can be obtained from SDSS broadband photometry accounting for the full flex of the galaxy and thus presumably the total stellar mass of the galaxy. The methodology and the motivations behind it are discussed in further detail in Section 2.2.3.

It follows from the above that the MPA-JHU catalog stellar masses would be systematically affected whenever the central M/L ratios were not representative of the entire galaxy. For example, the bulge and disk components of luminous spiral galaxies have systematically different star formation histories and thus mass-to-light ratios; since the bulge dominates

the inner part of the galaxy, it can potentially dominate the fiber spectrum and yield a M/L unrepresentative of the galaxy as a whole. To quantify exactly how this systematic affects MPA-JHU masses spatially resolved spectra for galaxies is necessary. Integral Field Unit (IFU) based surveys provide us the necessary data to be able to do that. In the following section, I review briefly the field of integral field spectroscopy and describe in more detail the MaNGA survey (Bundy et al., 2014).

2.1.3   Integral Field Spectroscopy and MaNGA

Integral Field Spectroscopy in astronomy is motivated by the need to study the variation of spectra across extended objects, in order to determine its internal structure and dynamics. An Integral Field Unit (IFU) enables the observation of multiple regions of the extended object simultaneously to obtain these spatially resolved spectra. There are many ways of doing this, including and not limited to image slicers, lenslet arrays, and multi-fiber IFUs. As we have seen in Section 2.1.1, while spectroscopic surveys have created huge breakthroughs in galaxy evolution and cosmology alike, their restricted spatial coverage has resulted in the need for more or less uncertain aperture corrections to measure properties of the galaxy as a whole, and in the inability to make reliable inferences about galaxies' internal structure.

Some noteworthy IFU-based surveys include the Sydney-Australian-Astronomical-Observatory Multi-object Integral-Field Spectrograph (SAMI; Bryant et al. 2015), the Multi Unit Spectroscopic Explorer (MUST; Bacon et al. 2015), and the Calar Alto Legacy Integral Field Area Survey (CALIFA; Sánchez et al. 2012). Over the last decade these and other surveys have contributed greatly to our understanding of the internal lives of galaxies. For the purposes of this project, the survey that bests suits our purposes is MaNGA (Mapping

Nearby Galaxies at Apache Point (Bundy et al., 2014)). MaNGA is the largest IFU-based survey undertaken so far in terms of numbers of galaxies, planning to obtain spatially resolved spectra of about 10,000 galaxies by 2020. This size and the homogeneous selection of galaxies is one important consideration (Section 2.3.1). Another important consideration is that it uses the BOSS spectrograph, which is very similar to the original SDSS spectrograph, and the data is calibrated and processed using very similar methods to SDSS-I and -II data. These properties make it a natural sample to use to test systematics in the methods applied to the MPA-JHU catalog.

MaNGA uses 17 multiple fiber IFUs simultaneously (Drory et al., 2015). In the same way that single fibers are plugged into plates (Section 2.1.1), the multiple fiber bundles are plugged at the appropriate locations on plug-plates to be observed at the focal plane of the 2.5m telescope at Apache Point. The fibers are 2.0″ in size and the bundles themselves come in five sizes and contain 19, 37, 61, 91 or 127 fibers. The bundle assigned to each galaxy is determined from the angular size of the target galaxy.

The fibers are arranged in a hexagonal pattern, and several observations are taken slightly offset from each other ("dithered") to produce a denser hexagonal sampling. During data processing, the observations are interpolated onto a rectangular grid at each wavelength. Each grid point is called a spaxel, which can be thought of as a spectrum for every two-dimensional pixel. The resulting MaNGA galaxy outputs are thus three dimensional "datacubes" with two spatial dimensions and one spectral dimension.

Each bundle also contains sky fibers to allow for very precise sky subtraction by looking at a region of the sky that is within a few arcminutes of the target. At a given time, MaNGA is able to target 17 galaxies (and 12 standard stars) in the 3 degree FOV with much wider and

continuous wavelength coverage than other large IFU-based surveys.

2.2 THE $H\delta_A - D_n4000$ PLANE

In this section, I review the two spectral diagnostic tools used by the MPA-JHU catalog to constrain stellar masses and star formation histories in galaxies, the Balmer δ absorption line index and the D_n4000 break index in the optical spectrum of a galaxy. Following that I describe the method used by Kauffmann et al. (2003) to obtain the mass-to-light ratios of galaxies using these indices and finally the aperture correction method used to tranform the fiber masses obtained to the total stellar mass of the galaxy.

2.2.1 THE D_n4000 BREAK IN GALAXY SPECTRA

Spectral discontinuities in stars can be produced by the accumulation of a large number of spectral lines in a narrow region. In certain cases this can lead to a relatively sharp discontinuity, or "break," in the spectrum of the star. A prominent break in galaxy spectra occurs in the optical at 4000 Å(Bruzual A., 1981; Bruzual A., 1983a), which exists in the spectra of K stars and thus appears in stellar populations older than a few billion years, which are dominated by K giants. Because it is associated with this late stage in the evolution of stellar populations, the strength of this break is an indicator of the mean stellar age over the past few billion years.

The specific metallic absorption lines causing the break include a variety of elements in varying states of ionization, including including the CaII doublet, H and K (3969 Åand 3934 Å) (Hamilton, 1985). The stellar break strength correlates positively with stellar metallicity, which means that for galaxies the break exhibits some of the same age-metallicity de-
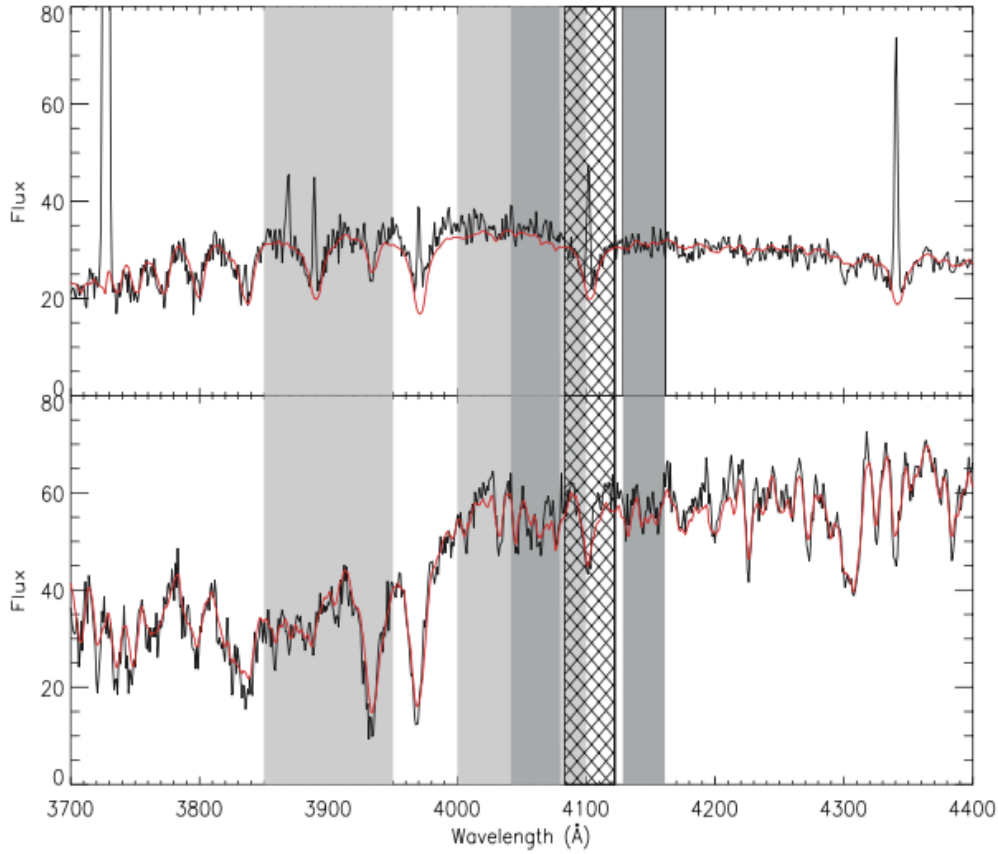
Figure 2.1: PLACEHOLDER FIG; TBD: A figure showing D4000 and Hdelta breaks in spectra for early/late-type galaxies as well as the bimodality in D4000

generacy that afflicts most spectroscopic indicators.

This break was defined in by Bruzual A. (1983b) as the ratio of the average flux density F_v in two bands that span ~200 Å on either side of 4000 Å. Balogh et al. (1999) defined a narrow bandwidth for the break (known as D_n4000), using 100 Å wide bands for the blue (3850–3950 Å) and red (4000–4100 Å). Kauffmann et al. (2003) (Figure 2.1) uses D_n4000, because it is less sensitive to dust reddening effects. In this section, I will use the same narrow band definition.
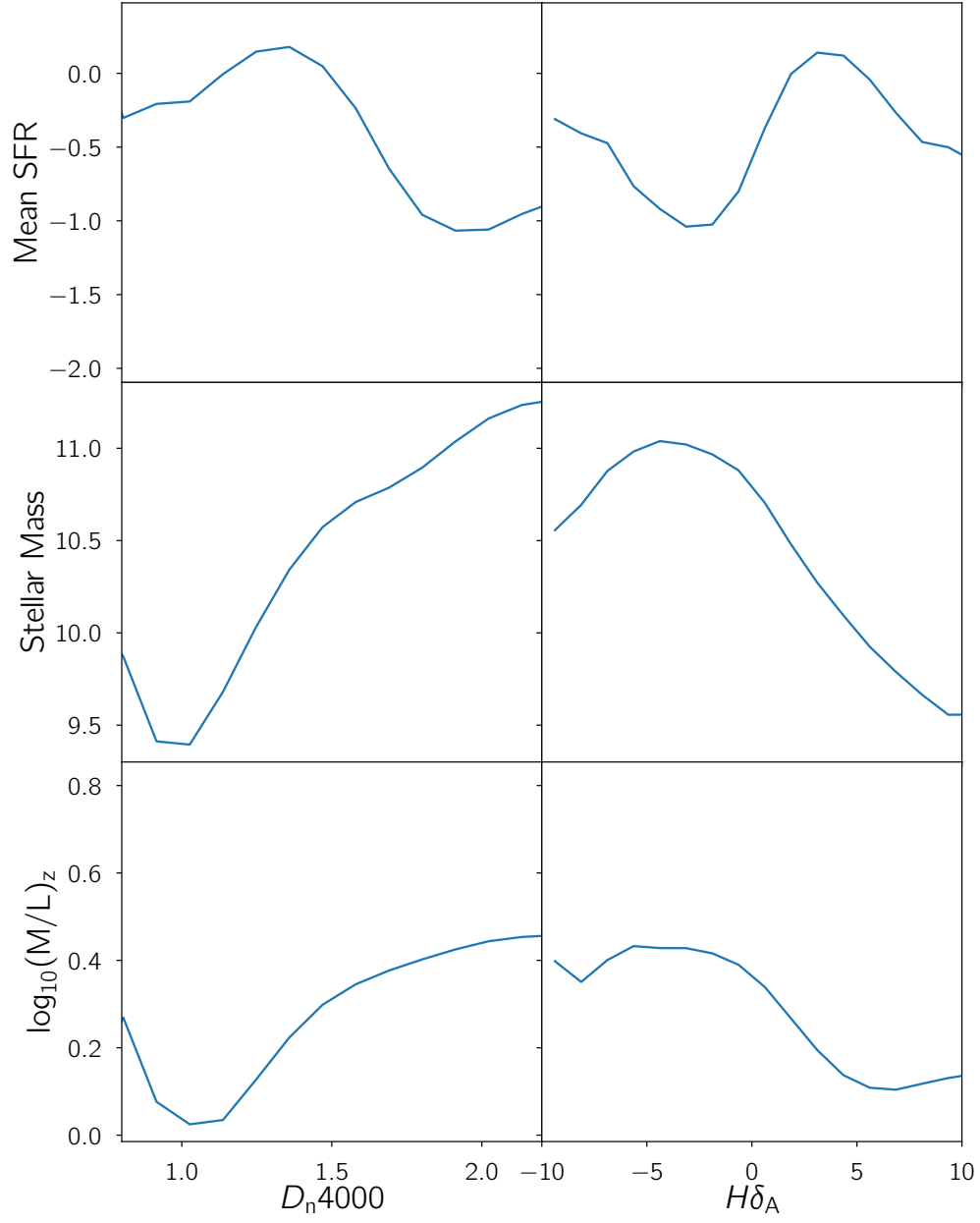
Figure 2.2: Stellar masses, ages and Mass-to-light ratios as a function of $H\delta_A$ and D_n4000 for the DR8 SDSS galaxies:
Age needs to be included

2.2.2 The Balmer Hδ Absorption Line

As we have seen in Section 0.3.2, the spectral features of galaxies contain a wealth of information about their star formation properties. In stellar populations, the Balmer absorption lines (Hα, Hβ, $H\gamma$, $H\delta$, ...) are indicative of the presence of A stars. The surface temperatures of these stars are cool enough that their photospheres are not fully ionized, but hot enough that the $n = 2$ state of hydrogen is populated and thus the $2 \rightarrow n$ transitions can cause absorption lines. The lifetimes of A stars are 0.5–1 billion years, and therefore the strength of the Balmer lines in galaxies is indicative of the relative fraction of star formation that has occurred in the past few hundred million to a billion years. For example, very strong Hδ absorption in the absence of signatures of star formation indicates a a starburst having happened and ended 0.5–1.5 Gyrs ago (Dressler & Gunn, 1983).

Like many spectroscopic indicators, because the temperature of the stars is negatively correlated with metallicity, Balmer line indicators also suffer from an age-metallicity degeneracy. However, this degeneracy can be broken with additional measurements of other features of the spectrum which have age-metallicity degeneracies that differ in detail. Thus with the appropriate SPS models, both the mean age and metallicity can be simultaneously obtained. The traditional tool for this purpose is the set of Lick indices, obtained by using stellar spectra from the Lick Observatory (Worthey, 1994; Worthey & Ottaviani, 1997). The Lick indices are a system of 25 line indices, whose relationship to underlying stellar properties is thought to be known.

Here we will utilize these index measurements of the Balmer lines. Specifically we focus on Hδ. Although this absorption line is weaker than the lower order lines, it is less contaminated. The interstellar gas in galaxies is emitting Balmer recombination lines. For Hα, β,

and γ, the emission can be strong enough to swamp the absorption line in the continuum.

Measuring these absorption feature indices involves measuring the flux in a central band-pass relative to two pseudo-continuum bandpasses on either side. The continuum from which the equivalent width is measured is defined by linear interpolation between the midpoints of the two flanking pseudo-continuum bandpasses. The bandpass definitions we use here, as defined by Worthey (1994) are: an index bandpass from 4083.50–4122.25 Å with the blue and red bandpasses on either side being 4041.60–4079.75 Å and 4128.50–4161 Å respectively.

2.2.3 Constraining SFH's using $H\delta_A$ and D_n4000

The MPA-JHU measurements of stellar masses and ages rely on the results concerning the evolution of the $H\delta_A$ and D_n4000 indices for stellar populations. The evolutionary tracks of these indices with age are mapped by the spectral library, STELIB, incorporated into the SPS models (Bruzual & Charlot, 2003a) that are used to fit the SDSS spectral data. A significant prediction of these models here is that D_n4000 is sensitive to the mean star formation rate over time scales of billions of years, whereas the $H\delta_A$ feature is sensitive to the mean star formation rate over hundreds of millions of years. These features therefore provide constraints on the star formation histories of the galaxies.

These observables are also related to metallicity, which means that how they relate to star formation history is affected by the age-metallicity degeneracy. However, the stellar mass-to-light ratio is also affected by this degeneracy in a similar fashion; therefore a given value of these observables tends to correspond to the same M/L even for different metallicity populations.

Kauffmann et al. (2013) exploit these properties to constrain the stellar mass-to-light ratios of galaxies by using a Bayesian inference technique. The prior distribution is a library of models that are generated by Monte Carlo realizations that are representative of both bursty and continuous star formation histories. The library consists of 32000 different star formation histories, and provides predictions for each of the $H\delta_A$ and D_n4000 indices, the stellar mass-to-light ratios in the z-band, the $g - r$ and $r - i$ colors, and the fraction of stellar mass formed in bursts over the past 2 Gyr.

This library of models thus enables the construction of a "model grid" in the $H\delta_A$-D_n4000 plane, where each point on the grid corresponds to a distribution of physical properties of the models. For each galaxy in SDSS DR8, the spectral indices are measured, and then the physical properties and their uncertainties inferred from the distribution corresponding to those spectral index values. The resulting median value of the posterior probability distributions of the parameters for each galaxy is then used as the "best" estimate in the catalog. The resulting mass-to-light ratios for the SDSS DR8 galaxies in the $H\delta_A$-D_n4000 plane thus obtained are plotted in Figure 2.3.

2.2.4 The Stellar Mass Aperture Bias in MPA-JHU

As we have reviewed in Section 2.1.1, the SDSS spectra collect starlight within the $3''$ fiber diameter, with fibers that have been placed as close to the centre of a galaxy as possible. Thus mass-to-light ratios discussed above only strictly apply to the center of the galaxies. To obtain total stellar masses, the MPA-JHU catalog applies the mass-to-light ratio to the z-band photometry, using a spectroscopically-determined correction for dust extinction. These procedures assumes that the fiber mass-to-light ratios and dust attenuation factor is applica-
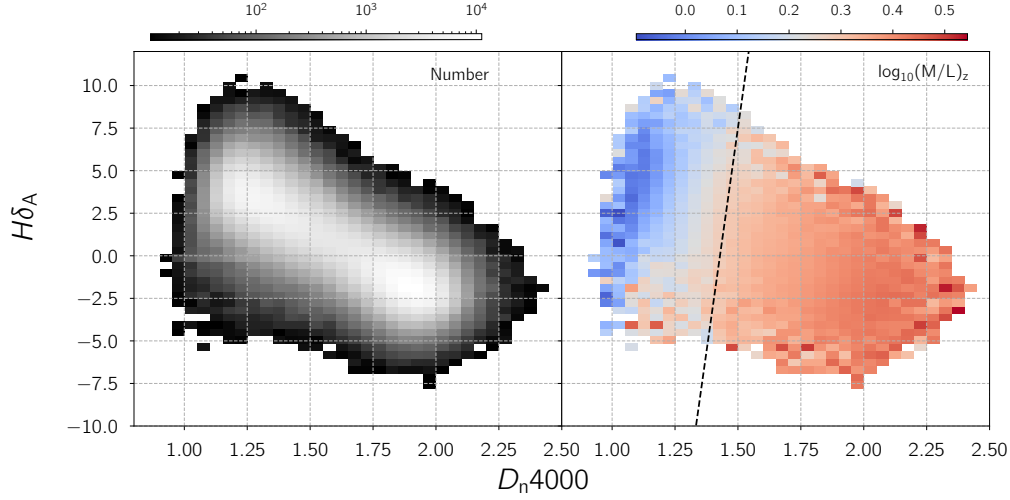
Figure 2.3: The Kauffmann et al. (2003) grid to infer M/L ratios from the $h\delta_A - D_n4000$ plane

ble to the whole galaxy. This assumption could in principle be a source of systematic error, i.e. an aperture bias, as discussed in Kauffmann et al. (2003) (and Brinchmann et al. (2004) for the star formation rates).

For example, spiral galaxies with star forming outer discs could have the index measurements in the central bulge not reflective of the galaxy's star formation properties as a whole at all.

Kauffmann et al. (2003) attempt to address this bias by comparing galaxies with similar z-band luminosities at different redshifts, using the fact that the physical size of the aperture will depend on distance, to see how significant the shift in D_n4000, $(M/L)_z$ and A_z are. They find that D_n4000 and A_z show a marked trend with redshift for galaxies whose absolute magnitude in z-band is between $-22.5 < M_z < -22.0$ but not for the galaxies that are brighter or fainter than that. The trends for $(M/L)_z$ are similar but less pronounced.

However, even at the outer limit of the redshifts probed, the median fraction of total light from a galaxy entering the fiber is only half the total, and so bias in the true global $(M/L)_z$ of the galaxies in the catalog is not measured by this technique.

The stellar mass estimates in the MPA-JHU catalog are certainly affected by other systematic effects, most prominently the choice of the stellar IMF (which can cause a factor of two issue), but also the stellar population model choice, the choice of the star formation history prior (i.e., the model library), and other effects. These sorts of biases have been explored in detail by other researchers (see Conroy 2013 and references therein). However, before this work there was not yet a direct demonstration that the aperture bias in these estimates was tolerable.

IFU-based surveys that cover a large fraction of each galaxy's area are ideal to test the aperture effects on both SFRs and stellar masses in the MPA-JHU catalog. Therefore, in this chapter I investigate the aperture effects on the stellar mass estimates by using spatially resolved spectral data from MaNGA.

2.3   Data and Methods

2.3.1   MaNGA Target Selection

We use the MaNGA data set for two reasons. First, its spectra have very similar properties to that of the original SDSS sample, with similar wavelength ranges and resolution. Second, its IFU data covers a large fraction of each galaxy, typically yielding a more global picture of each galaxy than obtainable from other surveys.

The MaNGA target selection is based on NSA photometry of SDSS Main Sample galaxies. The selection is designed to sample in a recoverable way as a function of stellar mass and

redshift, that in combination with the chosen fiber bundle sizes provide sufficient radial coverage as described in the next paragraph. The optimization process used to do this is described in Wake et al. (2017). MaNGA's goal is to observe approximately 10,000 galaxies by mid-2020, the end of SDSS-IV.

MaNGA radial coverage goals are to cover the galaxy well beyond its effective radius, R_e (the radius within which half of the galaxy's light is contained). There are three samples, the Primary, the Secondary, and the Color-enhanced samples. The Primary and Secondary samples, which make up 47% and 37% of the total sample, differ in the extent of spaxel coverage, with the former providing spectra for >80% of galaxies to beyond $1.5R_e$ and the latter providing spectra for >80% of galaxies to beyond $2.5R_e$. The cuts in redshift for both are chosen to ensure that there is a flat number density distribution of galaxies in the absolute i-band magnitude. The color-enhanced sample, which makes up about 16% of MaNGA, fills in for the undersampled regions in the N-i-M_i plane by extending the redshift limits in the primary sample so that galaxy types such as red galaxies with low luminosity, the green-valley galaxies and the high luminosity star-formers are better represented in MaNGA.

2.3.2   OUR SAMPLE

We use MaNGA Product Launch 8 (MPL-8), announced in November 2018, containing products based on galaxy and stellar library observations from March 2014 through July 2018. It contains 950 plates with 6779 galaxy data cubes. Out of these cubes, 6468 are galaxies with measured NSA redshifts. These are representative of all the IFU sizes (19, 37, 61, 91 or 127 fibers per IFU) and span a redshift range up to $z = 0.15$.

For each galaxy observation, depending on the IFU bundle size, the MaNGA Data Red-

shift Pipeline (Law et al. 2016) creates a data cube with spectra on a rectilinear grid with a spacing of 0.5″, with each grid point known as a "spaxel." The dimensions of the grid are aligned with north (Y) and east (X) on the sky.

2.3.3 Variable Aperture Measurements

For any given data cube, we want to convert it into a set of aperture spectra to simulate the spectra that the SDSS-I and -II surveys would have observed through single 3″ fibers at a given set of redshifts.

For any aperture radius R, we determine which spaxels fall within an aperture radius of R arcseconds based on its angular distance from the cube center (which corresponds to the center of each galaxy). Then we sum the spaxels within radius R to obtain the equivalent spectrum. Alternatively we can sum all of the spaxels to obtain a "full aperture" measurement. Strictly speaking this aperture is of course not always full; however, for the required coverage of $1.5R_e$, typically 70%–80% of the light is included (with the lower number for de Vaucouleurs galaxies and the upper number for exponential galaxies; Graham & Driver 2005).

For any MaNGA galaxy at redshift z_{obs}, we can simulate what the SDSS Main Sample spectrum would have looked like if it had observed the galaxy at that redshift or any higher redshift. We simply calculate the spectrum within an aperture that is 3″ diameter (if we are simulating the Main Sample spectrum at z_{obs}) or larger (if we are simulating the spectrum at a larger z). The transverse angular distance varies with redshift as follows:

$$D_{\mathrm{A}}(z) = \frac{D_{\mathrm{M}}(z)}{1 + z},$$

where $D_M(z)$ is the co-moving distance at redshift z. So when a galaxy at z_{obs} is shifted to some other z_{new} the new distance d_{new} of spaxel (x, y) from the central spaxel (x_c, y_c) relates to the old distance thus:

$$d_{new} = \frac{(1 + z_{new}) \times D_M(z_{obs}) \times d}{(1 + z_{obs}) \times D_M(z_{new})}$$

This equation allows us to define a new aperture of $d_{new} < 3''$.

For any spectral measurement we can then compare the measurement of the total spectrum in the MaNGA cube to that which would have been measured through a $3''$ aperture at a given redshift. Since galaxies come in a range of sizes and spectral profiles, this difference will vary from galaxy to galaxy and we must look at a large sample. Importantly, for a chosen redshift z_{new} at which to evaluate the degree of bias, we can only use a sample of galaxies with $z_{obs} \leq z_{new}$.

I measure $H\delta_A$ and D_n4000 indices in the standard fashion in the galaxy rest frames. To perform the measurements more efficiently, for each spaxel I measure the $H\delta_A$ central and side bands and the two D_n4000 bands, and store these five numbers separately. Then, instead of needing to access and coadd the full spectra, for each aperture I only need to add each of these five numbers across the relevant spaxels. I then combine them into the two index measurements following the procedure in Section 2.2.
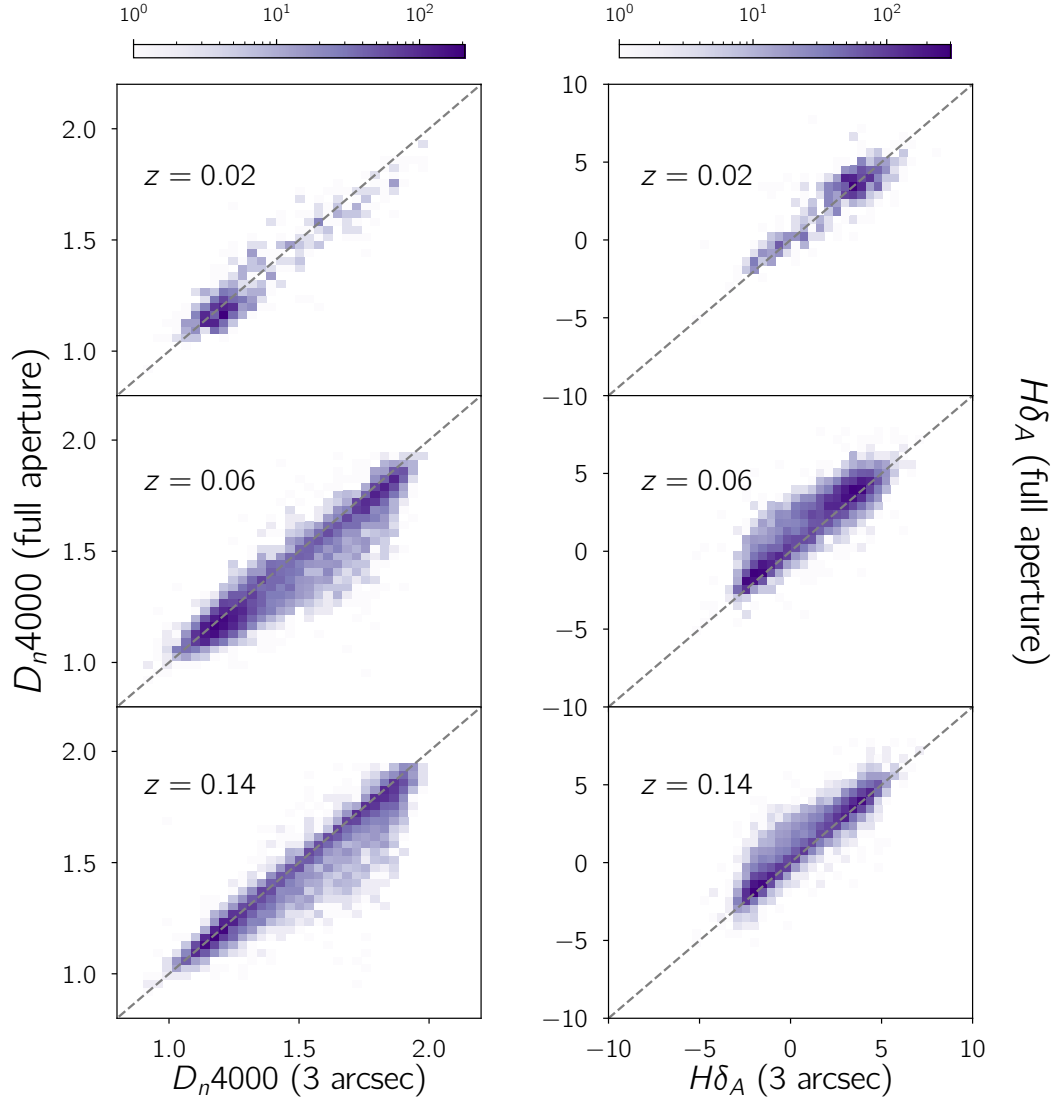
Figure 2.4: The D_n4000 and $H\delta_A$ indices measured at $z = 0.02$, 0.06, and 0.14 with a $3''$ aperture compared to the full aperture measurement. The dashed line corresponds to $x = y$.

2.4 RESULTS

2.4.1 COMPARISON TO FULL APERTURE MEASUREMENTS

To investigate how the full aperture measurements compare to the $3''$ measurements, I choose 3 different redshift bins $z = 0.02$, 0.06, and 0.14, and determine how offset the $H\delta_A$ and D_n4000 measures are. For each redshift z, I pick the galaxies with redshifts $z_{\text{obs}} < z$, "shift" them to the cutoff redshift as described in Section 2.3.3, and compare the full aperture measurements to the $3''$ measurements that would be made at redshift z.

The results of this procedure are shown in Fig. 2.4, where the full aperture measurements are plotted against the $3''$ measurements at the each redshift, with the colorbars indicating the number of galaxies in each bin. We note that the total number of galaxies at each redshift is 561 for $z = 0.02$, 5016 for $z = 0.06$ and 6402 for $z = 0.14$.

We first note the systematic change in the MaNGA sample between $z \sim 0.02$ and $z \sim 0.14$, which is related to MaNGA's target selection procedure. In order to achieve the desired areal coverage, MaNGA's selection of galaxies is such that the lower redshift galaxies are lower luminosity and mass. These lower luminosity galaxies are more star forming and have older stellar populations, so they have deeper $H\delta_A$ and weaker D_n4000. This trend is apparent in the variation in the galaxy population from panel to panel. This trend means we need to look at all of the panels to understand the comparison between $3''$ aperture and full aperture measurements of these quantities.

From Fig. 2.4, we can infer the following. For many galaxies the offset is pretty minimal; they fall pretty close to the $x = y$ line. The scatter is largest at $z = 0.06$, and this scatter tends towards higher D_n4000 and lower $H\delta_A$ values relative to the full aperture measure-
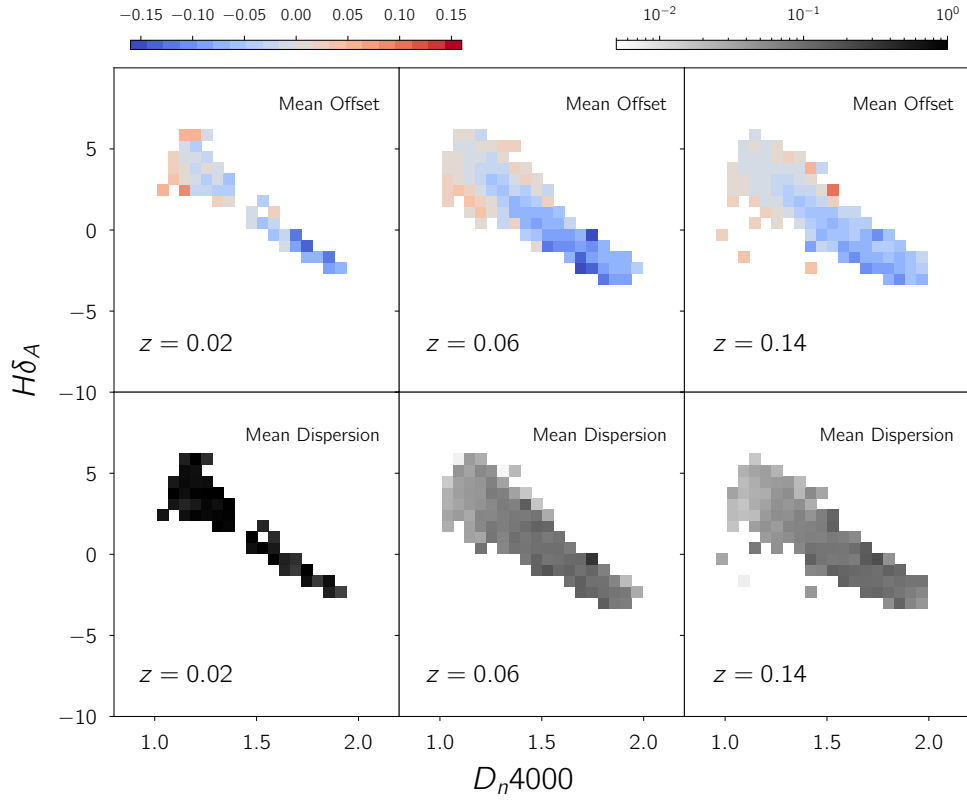
Figure 2.5: The mean offset and dispersion in the D_n4000 index measured at $z = 0.02, 0.06$ and 0.14 with a $3''$ aperture from the full aperture measurement
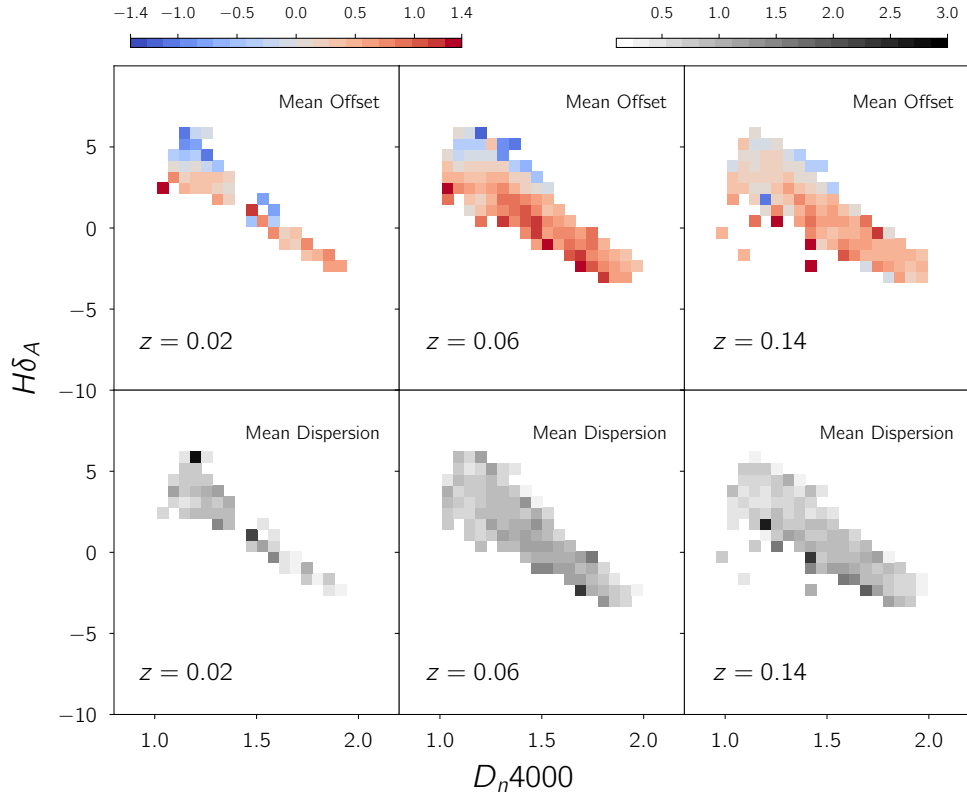
Figure 2.6: The mean offset and dispersion in the $H\delta_A$ index measured at $z = 0.02$, 0.06 and 0.14 with a $3''$ aperture from the full aperture measurement.

ments, particularly for galaxies with intermediate D_n4000 and $H\delta_A$ values for the full aperture. This effect is likely due to spiral galaxies with strong galactic bulges. These galaxies are common at the masses populating the $z_{obs} < 0.06$ bin, and have the property that their bulges are considerably less star-forming than their disks. Thus, the $3''$ aperture might cover their bulge but not their disk, and therefore show higher D_n4000 and lower $H\delta_A$ than the full aperture measurement. This effect is less prominent at $z = 0.02$ because the galaxies in the MaNGA sample at those redshifts are lower luminosity and have less prominent bulges. The scatter also lessens as we approach $z = 0.14$, close to the survey limit; although this sample also contains spirals with strong bulges, the $3''$ aperture is larger with respect to the total size of galaxies at this redshift.

From this figure, we conclude generally that the restrictions of how the MaNGA sample is selected make it hard to evaluate the effects of the aperture bias at the lowest redshifts ($z \sim 0.02$) — clearly the sample there is not representative of the sample as a whole. However, the $z = 0.06$ and $z = 0.14$ cases bracket the median redshift of the SDSS Main Sample so will characterize the aperture bias well for much of that sample. We can guess already that the general effect will be that the $3''$ fiber will overestimate the stellar ages and therefore their mass-to-light ratios, for some fraction of the galaxies.

2.4.2 OFFSETS IN THE $H\delta_A$-D_n4000 PLANE

The next step in comparing the full aperture measurements to the $3''$ measurements is to determine where the galaxies move in the $H\delta_A$ - D_n4000 plane for each of the redshift bins. We bin the galaxies according to the $3''$ measurements in both D_n4000 and $H\delta_A$, and measure the mean and standard deviation within each bin of the offsets between the $3''$ and full
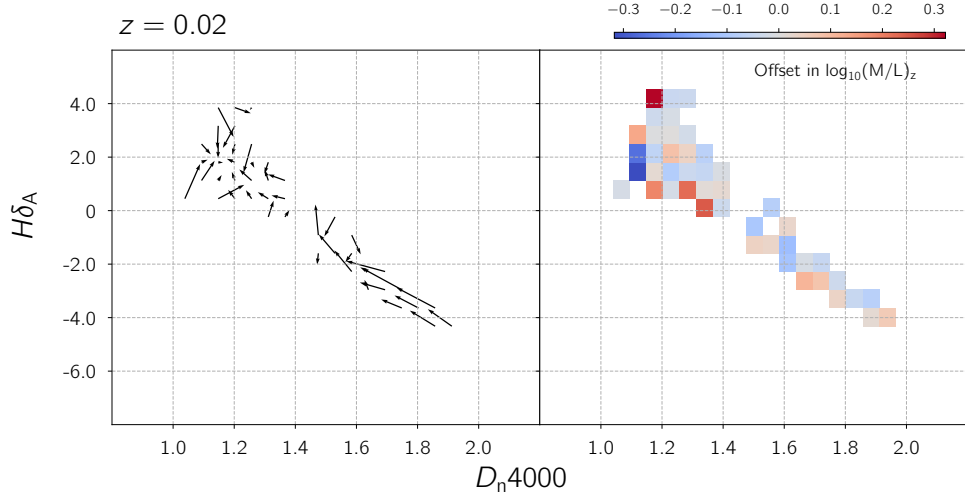
Figure 2.7: *Left:* The combined mean offset in D_n4000-$h\delta_A$ at $z = 0.02$ from the full aperture measurements represented as a vector whose projections on the axes are the actual offsets in either direction. *Right:* The offsets transformed to the z-band mass-to-light ratios using the grid in Figure 2.3.
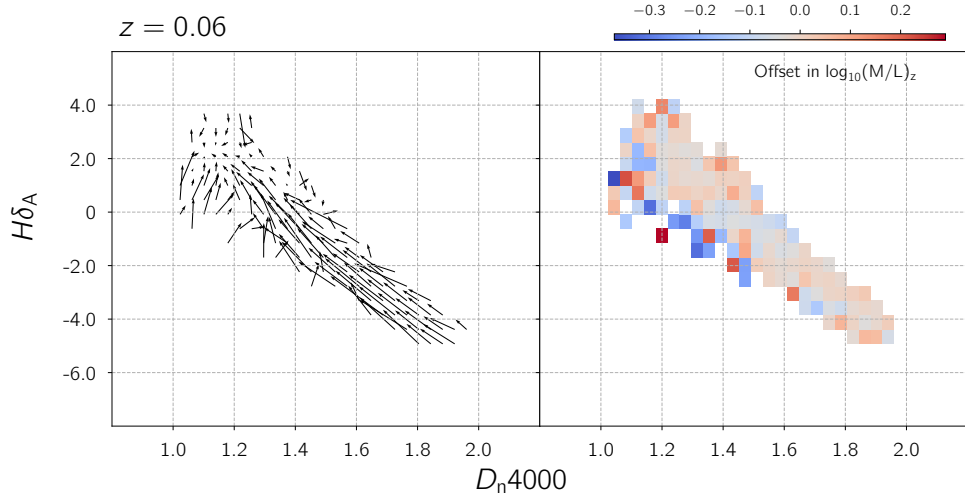
Figure 2.8: *Left:* The combined mean offset in D_n4000-$h\delta_A$ at $z = 0.06$ from the full aperture measurements represented as a vector whose projections on the axes are the actual offsets in either direction. *Right:* The offsets transformed to the z-band mass-to-light ratios using the grid in Figure 2.3.
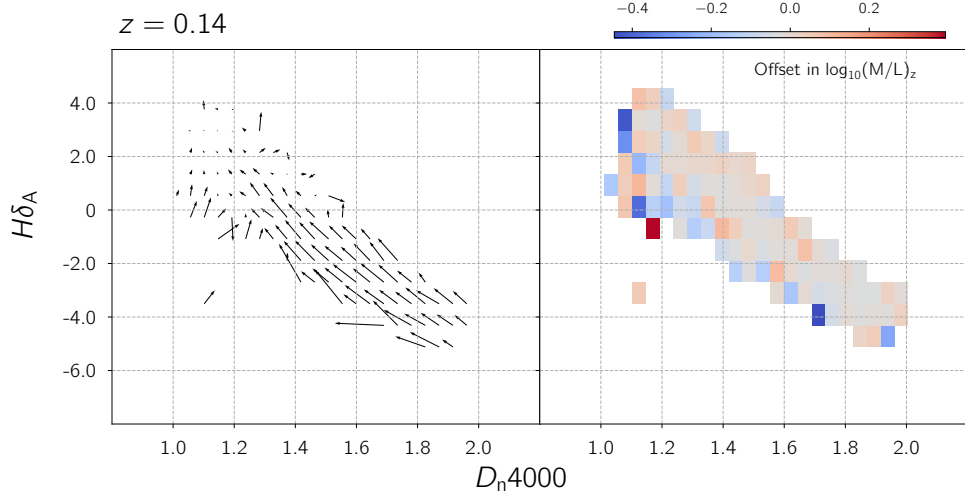
Figure 2.9: *Left:* The combined mean offset in D_n4000-$h\delta_A$ at $z = 0.14$ from the full aperture measurements represented as a vector whose projections on the axes are the actual offsets in either direction. *Right:* The offsets transformed to the z-band mass-to-light ratios using the grid in Figure 2.3.

aperture measurements. Figure 2.5 shows the mean offsets and standard deviations for the D_n4000 measurements. Figure 2.6 shows the mean offsets and standard deviations for the $H\delta_A$ measurements. The general tendency we see in the D_n4000 offsets is that the older galaxies tend to have slightly negative offsets and the younger ones tend to have slightly positive offsets. In the case of $H\delta_A$, the offsets on average tend to be mostly positive (in this case, tending toward the region of phase space with younger galaxies) with the exception of a few bins with high $H\delta_A$ where there are a few small negative offsets.

The combined offsets in both the directions are plotted as quiver plots that occupy the left subplots in Figures 2.7, 2.8 and 2.9. The length of the vector offsets in the quiver plots can translate into very different offsets in $\log_{10}((M/L)_z)$ depending on where they occur in the $H\delta_A$ - D_n4000 plane. Using the MPA-JHU mass-to-light ratios and index measure-

	Mean M/L Ratio (below)	Mean Offset (below)	Dispersion (below)	Mean M/L Ratio (above)	Mean Offset (above)	Dispersion (above)
$z = 0.02$	0.36	-0.021	0.217	0.094	0.004	0.324
$z = 0.06$	0.361	-0.027	0.181	0.121	-0.025	0.267
$z = 0.14$	0.366	-0.018	0.18	0.118	-0.014	0.251

Figure 2.10: Table showing the mean offsets for the three redshift bins

ments for SDSS DR8 galaxies, we have reconstructed the transformation from a $(D_n4000,$ $H\delta_A)$ value to a $\log_{10}((M/L)_z)$ value by interpolating the grid shown in Figure 2.3. Thus each offset in the plane can be converted to an offset in terms of the mass-to-light ratios. These mass-to-light ratio offsets are plotted in the right subplots in the aforementioned figures.

Figure 2.11 summarizes these findings, showing the mass-to-light ratio offset and standard deviation in each bin for each redshift. We quantity these findings in Tables 2.10 and 2.12. For these tables, we evaluate the mean and median offsets and the standard deviations for the older and younger galaxies, separated using the cut in the D_n4000-$h\delta_A$ plane shown in Figure 2.3. Table 2.12 also gives the median absolute deviation; these median absolute deviations are smaller (by about 50%) than would be expected for a Gaussian distribution given the standard deviations, indicating that the distributions have a somewhat longer tail to extreme values than Gaussian.
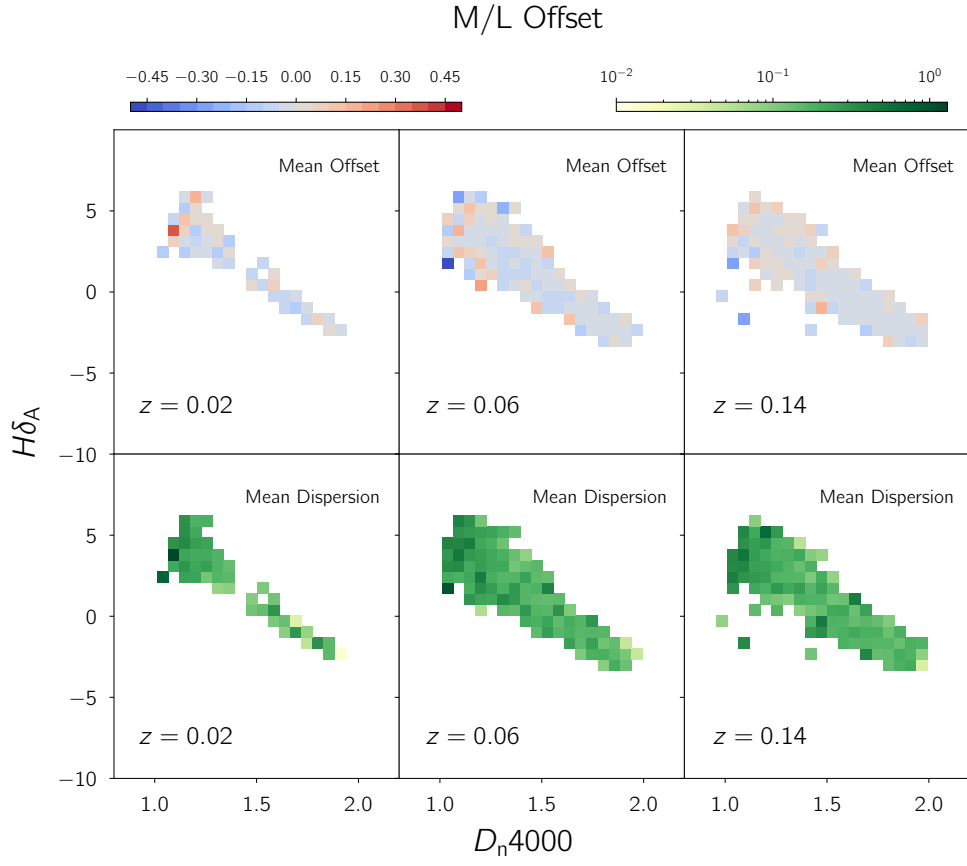
Figure 2.11: The mean and dispersions of the mass-to-light ratio offsets in each of the redshift bins.

	Median M/L Ratio (below)	Median Offset (below)	Median AbsDev(below)	Median M/L Ratio (above)	Median Offset (above)	Median AbsDev (above)
$z = 0.02$	0.385	-0.031	0.07	0.095	-0.011	0.155
$z = 0.06$	0.371	-0.023	0.08	0.13	-0.031	0.14
$z = 0.14$	0.38	-0.01	0.074	0.131	-0.004	0.123

Figure 2.12: Table showing the median offsets for the three redshift bins

2.5 Discussion

The results above lead us to the following conclusions:

- The mean mass-to-light ratio offset for all galaxies is relatively small. Both Table 2.10 and Figure 2.11 show that for both the younger and older galaxies in all bins, there is a slight negative mean and median offset.

- The scatter about the mean is substantial relative to the mean. For the mid-redshift bin, the standard deviation for the older galaxies is ~ 0.181 and for the younger galaxies is ~ 0.267. These relatively large standard deviations imply that for individual galaxies, the effect of aperture bias large even if the average trend is small. This is also reflected in the uniformly high dispersions across bins in Figure 2.11.

The fact that the mean offsets from the the full aperture measurements are small implies that the mean MPA-JHU masses are robust. These measurements are therefore not likely to cause an overall shift in the measured stellar mass function, for example.

However, the standard deviations are interestingly large. The scatter this result implies in the stellar mass function is interesting for several reasons. First, it implies a correlation between the stellar mass systematic error and the structure of galaxies, implying that galaxies with stronger bulges will have a slightly larger estimated mass. The standard deviation of 0.2 dex is still small relative to the stellar mass bins defined by many analyses, but near the steep slope of the stellar mass function at high masses it may cause problems.

Second, this standard deviation, though small, is close to the standard deviation inferred between halo mass and stellar mass for massive galaxies. For example, for BOSS galaxies (which are further away and therefore less prone to aperture effects) Tinker et al. 2017 find around $\sim$ 0.2 dex standard deviation of stellar mass at fixed halo mass based on their clustering. This result implies that a systematic error causing a 0.2 dex standard deviation (even with a mean of zero) is enough to affect similar analyses based on spectroscopic measurements with the SDSS Main Sample, and therefore is a potential cause of concern for some applications.

Lastly, and related to both the previous points, this 0.2 dex standard deviation can affect the massive end of the stellar mass function, causing the exponential cutoff at high masses to be less suddent than in reality.

In general, the results here suggest that some care may need to be taken in some contexts using the widely applied Kauffmann et al. (2003) results. Tables 2.10 and 2.12 and Figure 2.11 yield the quantitative description necessary to determine in which contexts these effects become important. Exactly how to account for them will depend on the population of galaxies being studied, in particular their redshift, color, and mass selection.

A similar set of concerns may affect the Brinchmann et al. (2004) results in the MPA-

JHU catalog regarding star formation rates. These effects can be estimated using techniques similar to those I use here.

3

Conclusion

In this thesis I have successfully explored two aspects of calibrating star formation indicators. In Chapter 1, I have examined one of the most popularly used methods of star formation estimation that is purely dependent on UV emission and assessed how well it traces star formation in dusty galaxies and in Chapter 2, I have evaluated the effects of aperture bias in the stellar masses estimated at the largest star formation and stellar mass catalog of

galaxies, the MPA-JHU catalog. The need for calibrating observational indicators of star formation indicators and investigating the systematic errors they might have has been discussed in Chapter 0. In this section I will summarize and discuss the significance of both these results, where they would be applicable and the scope for further exploration in either area.

The significant results in Chapter 1 are that the UV based star formation rates are not efficient tracers of star formation, especially in the case of dusty star formers that reside in the optical "green valley" and that we need IR based calibrations to help us identify these dusty star formers much better. These conclusions were arrived at by looking at a purely UV-based star formation rate and a UV-to-IR based star formation rate for a sample of nearby galaxies and the latter was used to identify a distinct population of dust-obscured star formers in a color-color phase space. To confirm this identification, a third independent property, namely the environment of the galaxies was estimated and it was found that the environments of this population behaved more in alignment with star forming galaxies than passive, red and dead galaxies.

Since the advent of the space-based GALEX telescope, most high redshift surveys have relied heavily on UV-based star formation rates. These UV-based measurements have played an essential sole in mapping the cosmic star formation history of the Universe. My result however implies that UV based star formation rates fail in a non-trivial way in capturing dusty star formers and tend to categorize them as less star forming than what they really are. There is further scope for exploration of this and the corrections this would entail in the near future with the launch of the James Webb Space Telescope (JWST) which aims at getting long wavelength visible to mid-IR information for high redshift objects.

In Chapter 2, I have investigated the effect of aperture bias due to the 3" SDSS fiber in the stellar mass estimation method for the MPA-JHU catalog by making use of spatially resolved spectral data from the MaNGA IFU-based survey and reproducing the Kauffmann et al. (2003) method which relies to two key spectral indicators. And while the mean tendency in the offsets from full aperture measurements is small, the dispersion in the offsets across the phase space of the spectral indicators was found to be high, implying a correlation between the systematic error in stellar mass and a galaxy's morphology. In particular, it implies that the MPA-JHU method over-estimates the stellar mass of galaxies with strong bulges. Further, the implication of this for the halo masses inferred from stellar masses via abundance matching implies is a cause for concern while using the MPA-JHU masses. The method I used to investigate the aperture bias in the MPA-JHU masses can be similarly extended to the MPA-JHU catalog star formation rates as well. This form of aperture correction would be crucial for any fiber-based survey and in particular, for upcoming surveys like the DESI Bright Galaxy Survey, an exploration of the systematic effects of aperture bias on the estimation of galaxy properties in the same vein as mine can be immensely useful.

References

Agertz, O., Moore, B., Stadel, J., Potter, D., Miniati, F., Read, J., Mayer, L., Gawryszczak, A., Kravtsov, A., Nordlund, Å., Pearce, F., Quilis, V., Rudd, D., Springel, V., Stone, J., Tasker, E., Teyssier, R., Wadsley, J., & Walder, R. (2007). Fundamental differences between SPH and grid methods. *Monthly Notices of the Royal Astronomical Society*, 380, 963–978.

Aihara, H., Allende Prieto, C., An, D., Anderson, S. F., Aubourg, É., Balbinot, E., Beers, T. C., Berlind, A. A., Bickerton, S. J., Bizyaev, D., Blanton, M. R., Bochanski, J. J., Bolton, A. S., Bovy, J., Brand t, W. N., Brinkmann, J., Brown, P. J., Brownstein, J. R., Busca, N. G., Campbell, H., Carr, M. A., Chen, Y., Chiappini, C., Comparat, J., Connolly, N., Cortes, M., Croft, R. A. C., Cuesta, A. J., da Costa, L. N., Davenport, J. R. A., Dawson, K., Dhital, S., Ealet, A., Ebelke, G. L., Edmondson, E. M., Eisenstein, D. J., Escoffier, S., Esposito, M., Evans, M. L., Fan, X., Femenía Castellá, B., Font-Ribera, A., Frinchaboy, P. M., Ge, J., Gillespie, B. A., Gilmore, G., González Hernández, J. I., Gott, J. R., Gould, A., Grebel, E. K., Gunn, J. E., Hamilton, J.-C., Harding, P., Harris, D. W., Hawley, S. L., Hearty, F. R., Ho, S., Hogg, D. W., Holtzman, J. A., Honscheid, K., Inada, N., Ivans, I. I., Jiang, L., Johnson, J. A., Jordan, C., Jordan, W. P., Kazin, E. A., Kirkby, D., Klaene, M. A., Knapp, G. R., Kneib, J.-P., Kochanek, C. S., Koesterke, L., Kollmeier, J. A., Kron, R. G., Lampeitl, H., Lang, D., Le Goff, J.-M., Lee, Y. S., Lin, Y.-T., Long, D. C., Loomis, C. P., Lucatello, S., Lundgren, B., Lupton, R. H., Ma, Z., MacDonald, N., Mahadevan, S., Maia, M. A. G., Makler, M., Malanushenko, E., Malanushenko, V., Mandelbaum, R., Maraston, C., Margala, D., Masters, K. L., McBride, C. K., McGehee, P. M., McGreer, I. D., Ménard, B., Miralda-Escudé, J., Morrison, H. L., Mullally, F., Muna, D., Munn, J. A., Murayama, H., Myers, A. D., Naugle, T., Neto, A. F., Nguyen, D. C., Nichol, R. C., O'Connell, R. W., Ogando, R. L. C., Olmstead, M. D., Oravetz, D. J., Padmanabhan, N., Palanque-Delabrouille, N., Pan, K., Pandey, P., Pâris, I., Percival, W. J., Petitjean, P., Pfaffenberger, R., Pforr, J., Phleps, S., Pichon, C., Pieri, M. M., Prada, F., Price-Whelan, A. M., Raddick, M. J., Ramos, B. H. F., Reylé, C., Rich, J., Richards, G. T., Rix, H.-W., Robin, A. C., Rocha-Pinto, H. J., Rockosi, C. M., Roe, N. A., Rollinde, E., Ross, A. J., Ross, N. P., Rossetto, B. M., Sánchez, A. G., Sayres, C., Schlegel, D. J., Schlesinger, K. J., Schmidt, S. J.,

Schneider, D. P., Sheldon, E., Shu, Y., Simmerer, J., Simmons, A. E., Sivarani, T., Snedden, S. A., Sobeck, J. S., Steinmetz, M., Strauss, M. A., Szalay, A. S., Tanaka, M., Thakar, A. R., Thomas, D., Tinker, J. L., Tofflemire, B. M., Tojeiro, R., Tremonti, C. A., Vandenberg, J., Vargas Magaña, M., Verde, L., Vogt, N. P., Wake, D. A., Wang, J., Weaver, B. A., Weinberg, D. H., White, M., White, S. D. M., Yanny, B., Yasuda, N., Yeche, C., & Zehavi, I. (2011). The Eighth Data Release of the Sloan Digital Sky Survey: First Data from SDSS-III. *The Astrophysical Journal Supplement Series*, 193, 29.

Alpher, R. A., Bethe, H., & Gamow, G. (1948). The Origin of Chemical Elements. *Physical Review*, 73(7), 803–804.

Bacon, R., Brinchmann, J., Richard, J., Contini, T., Drake, A., Franx, M., Tacchella, S., Vernet, J., Wisotzki, L., Blaizot, J., Bouché, N., Bouwens, R., Cantalupo, S., Carollo, C. M., Carton, D., Caruana, J., Clément, B., Dreizler, S., Epinat, B., Guiderdoni, B., Herenz, C., Husser, T.-O., Kamann, S., Kerutt, J., Kollatschny, W., Krajnovic, D., Lilly, S., Martinsson, T., Michel-Dansac, L., Patricio, V., Schaye, J., Shirazi, M., Soto, K., Soucail, G., Steinmetz, M., Urrutia, T., Weilbacher, P., & de Zeeuw, T. (2015). The MUSE 3D view of the *Hubble* Deep Field South. *Astronomy & Astrophysics*, 575, A75.

Balogh, M. L., Morris, S. L., Yee, H. K. C., Carlberg, R. G., & Ellingson, E. (1999). Differential Galaxy Evolution in Cluster and Field Galaxies at z˜0.3. *The Astrophysical Journal*, 527, 54–79.

Behroozi, P. S., Conroy, C., & Wechsler, R. H. (2010). A COMPREHENSIVE ANALYSIS OF UNCERTAINTIES AFFECTING THE STELLAR MASS-HALO MASS RELATION FOR 0 < z < 4. *The Astrophysical Journal*, 717(1), 379–403.

Bell, E. F. & de Jong, R. S. (2001). Stellar Mass-to-Light Ratios and the Tully-Fisher Relation. *The Astrophysical Journal*, 550, 212–229.

Best, P. N., Kauffmann, G., Heckman, T. M., Brinchmann, J., Charlot, S., Ivezić, Ž., & White, S. D. M. (2005). The host galaxies of radio-loud active galactic nuclei: mass dependences, gas cooling and active galactic nuclei feedback. *Monthly Notices of the Royal Astronomical Society*, 362, 25–40.

Blanton, M. R., Bershady, M. A., Abolfathi, B., Albareti, F. D., Allende Prieto, C., Almeida, A., Alonso-García, J., Anders, F., Anderson, S. F., Andrews, B., Aquino-Ortíz, E., Aragón-Salamanca, A., Argudo-Fernández, M., Armengaud, E., Aubourg, E., Avila-Reese, V., Badenes, C., Bailey, S., Barger, K. A., Barrera-Ballesteros, J., Bartosz, C., Bates, D., Baumgarten, F., Bautista, J., Beaton, R., Beers, T. C., Belfiore, F., Bender, C. F., Berlind, A. A., Bernardi, M., Beutler, F., Bird, J. C., Bizyaev, D., Blanc, G. A., Blomqvist,

M., Bolton, A. S., Boquien, M., Borissova, J., van den Bosch, R., Bovy, J., Brandt, W. N., Brinkmann, J., Brownstein, J. R., Bundy, K., Burgasser, A. J., Burtin, E., Busca, N. G., Cappellari, M., Delgado Carigi, M. L., Carlberg, J. K., Carnero Rosell, A., Carrera, R., Chanover, N. J., Cherinka, B., Cheung, E., Gómez Maqueo Chew, Y., Chiappini, C., Doohyun Choi, P., Chojnowski, D., Chuang, C.-H., Chung, H., Cirolini, R. F., Clerc, N., Cohen, R. E., Comparat, J., da Costa, L., Cousinou, M.-C., Covey, K., Crane, J. D., Croft, R. A. C., Cruz-Gonzalez, I., Garrido Cuadra, D., Cunha, K., Damke, G. J., Darling, J., Davies, R., Dawson, K., de la Macorra, A., Dell'Agli, F., De Lee, N., Delubac, T., Di Mille, F., Diamond-Stanic, A., Cano-Díaz, M., Donor, J., José Downes, J., Drory, N., du Mas des Bourboux, H., Duckworth, C. J., Dwelly, T., Dyer, J., Ebelke, G., Eigenbrot, A. D., Eisenstein, D. J., Emsellem, E., Eracleous, M., Escoffier, S., Evans, M. L., Fan, X., Fernández-Alvar, E., Fernandez-Trincado, J. G., Feuillet, D. K., Finoguenov, A., Fleming, S. W., Font-Ribera, A., Fredrickson, A., Freischlad, G., Frinchaboy, P. M., Fuentes, C. E., Galbany, L., Garcia-Dias, R., García-Hernández, D. A., Gaulme, P., Geisler, D., Gelfand, J. D., Gil-Marín, H., Gillespie, B. A., Goddard, D., Gonzalez-Perez, V., Grabowski, K., Green, P. J., Grier, C. J., Gunn, J. E., Guo, H., Guy, J., Hagen, A., Hahn, C., Hall, M., Harding, P., Hasselquist, S., Hawley, S. L., Hearty, F., Gonzalez Hernández, J. I., Ho, S., Hogg, D. W., Holley-Bockelmann, K., Holtzman, J. A., Holzer, P. H., Huehnerhoff, J., Hutchinson, T. A., Hwang, H. S., Ibarra-Medel, H. J., da Silva Ilha, G., Ivans, I. I., Ivory, K., Jackson, K., Jensen, T. W., Johnson, J. A., Jones, A., Jönsson, H., Jullo, E., Kamble, V., Kinemuchi, K., Kirkby, D., Kitaura, F.-S., Klaene, M., Knapp, G. R., Kneib, J.-P., Kollmeier, J. A., Lacerna, I., Lane, R. R., Lang, D., Law, D. R., Lazarz, D., Lee, Y., Le Goff, J.-M., Liang, F.-H., Li, C., Li, H., Lian, J., Lima, M., Lin, L., Lin, Y.-T., Bertran de Lis, S., Liu, C., de Icaza Lizaola, M. A. C., Long, D., Lucatello, S., Lundgren, B., Mac-Donald, N. K., Deconto Machado, A., MacLeod, C. L., Mahadevan, S., Geimba Maia, M. A., Maiolino, R., Majewski, S. R., Malanushenko, E., Malanushenko, V., Manchado, A., Mao, S., Maraston, C., Marques-Chaves, R., Masseron, T., Masters, K. L., McBride, C. K., McDermid, R. M., McGrath, B., McGreer, I. D., Medina Peña, N., Melendez, M., Merloni, A., Merrifield, M. R., Meszaros, S., Meza, A., Minchev, I., Minniti, D., Miyaji, T., More, S., Mulchaey, J., Müller-Sánchez, F., Muna, D., Munoz, R. R., Myers, A. D., Nair, P., Nandra, K., Correa do Nascimento, J., Negrete, A., Ness, M., Newman, J. A., Nichol, R. C., Nidever, D. L., Nitschelm, C., Ntelis, P., O'Connell, J. E., Oelkers, R. J., Oravetz, A., Oravetz, D., Pace, Z., Padilla, N., Palanque-Delabrouille, N., Alonso Palicio, P., Pan, K., Parejko, J. K., Parikh, T., Pâris, I., Park, C., Patten, A. Y., Peirani, S., Pellejero-Ibanez, M., Penny, S., Percival, W. J., Perez-Fournon, I., Petitjean, P., Pieri, M. M., Pinsonneault, M., Pisani, A., Poleski, R., Prada, F., Prakash, A., Queiroz, A. B. d. A., Raddick, M. J., Raichoor, A., Barboza Rembold, S., Richstein, H., Riffel, R. A., Riffel, R., Rix, H.-W., Robin, A. C., Rockosi, C. M., Rodríguez-Torres, S., Roman-Lopes, A.,

Román-Zúñiga, C., Rosado, M., Ross, A. J., Rossi, G., Ruan, J., Ruggeri, R., Rykoff, E. S., Salazar-Albornoz, S., Salvato, M., Sánchez, A. G., Aguado, D. S., Sánchez-Gallego, J. R., Santana, F. A., Santiago, B. X., Sayres, C., Schiavon, R. P., da Silva Schimoia, J., Schlafly, E. F., Schlegel, D. J., Schneider, D. P., Schultheis, M., Schuster, W. J., Schwope, A., Seo, H.-J., Shao, Z., Shen, S., Shetrone, M., Shull, M., Simon, J. D., Skinner, D., Skrutskie, M. F., Slosar, A., Smith, V. V., Sobeck, J. S., Sobreira, F., Somers, G., Souto, D., Stark, D. V., Stassun, K., Stauffer, F., Steinmetz, M., Storchi-Bergmann, T., Streblyanska, A., Stringfellow, G. S., Suárez, G., Sun, J., Suzuki, N., Szigeti, L., Taghizadeh-Popp, M., Tang, B., Tao, C., Tayar, J., Tembe, M., Teske, J., Thakar, A. R., Thomas, D., Thompson, B. A., Tinker, J. L., Tissera, P., Tojeiro, R., Hernandez Toledo, H., de la Torre, S., Tremonti, C., Troup, N. W., Valenzuela, O., Martinez Valpuesta, I., Vargas-González, J., Vargas-Magaña, M., Vazquez, J. A., Villanova, S., Vivek, M., Vogt, N., Wake, D., Walterbos, R., Wang, Y., Weaver, B. A., Weijmans, A.-M., Weinberg, D. H., Westfall, K. B., Whelan, D. G., Wild, V., Wilson, J., Wood-Vasey, W. M., Wylezalek, D., Xiao, T., Yan, R., Yang, M., Ybarra, J. E., Yèche, C., Zakamska, N., Zamora, O., Zarrouk, P., Zasowski, G., Zhang, K., Zhao, G.-B., Zheng, Z., Zheng, Z., Zhou, X., Zhou, Z.-M., Zhu, G. B., Zoccali, M., & Zou, H. (2017). Sloan Digital Sky Survey IV: Mapping the Milky Way, Nearby Galaxies, and the Distant Universe. *The Astronomical Journal*, 154, 28.

Blanton, M. R., Eisenstein, D., Hogg, D. W., & Zehavi, I. (2006). The Scale Dependence of Relative Galaxy Bias: Encouragement for the "Halo Model" Description. *The Astrophysical Journal*, 645, 977–985.

Blanton, M. R., Hogg, D. W., Bahcall, N. A., Baldry, I. K., Brinkmann, J., Csabai, I., Eisenstein, D., Fukugita, M., Gunn, J. E., Ivezić, Ž., Lamb, D. Q., Lupton, R. H., Loveday, J., Munn, J. A., Nichol, R. C., Okamura, S., Schlegel, D. J., Shimasaku, K., Strauss, M. A., Vogeley, M. S., & Weinberg, D. H. (2003). The Broadband Optical Properties of Galaxies with Redshifts 0.02<z<0.22. *The Astrophysical Journal*, 594, 186–207.

Blanton, M. R., Kazin, E., Muna, D., Weaver, B. A., & Price-Whelan, A. (2011). Improved Background Subtraction for the Sloan Digital Sky Survey Images. *The Astronomical Journal*, 142, 31.

Blanton, M. R., Lupton, R. H., Schlegel, D. J., Strauss, M. A., Brinkmann, J., Fukugita, M., & Loveday, J. (2005). The Properties and Luminosity Function of Extremely Low Luminosity Galaxies. *The Astrophysical Journal*, 631, 208–230.

Blanton, M. R. & Moustakas, J. (2009a). Physical Properties and Environments of Nearby Galaxies. *Annual Review of Astronomy and Astrophysics*, 47(1), 159–210.

Blanton, M. R. & Moustakas, J. (2009b). Physical Properties and Environments of Nearby Galaxies. *Annual Review of Astronomy and Astrophysics*, 47(1), 159–210.

Blanton, M. R. & Roweis, S. (2007). K-Corrections and Filter Transformations in the Ultraviolet, Optical, and Near-Infrared. *The Astronomical Journal*, 133, 734–754.

Brinchmann, J., Charlot, S., White, S. D. M., Tremonti, C., Kauffmann, G., Heckman, T., & Brinkmann, J. (2004). The physical properties of star-forming galaxies in the low-redshift Universe. *Monthly Notices of the Royal Astronomical Society*, 351(4), 1151–1179.

Bruzual, G. & Charlot, S. (2003a). Stellar population synthesis at the resolution of 2003. *Monthly Notices of the Royal Astronomical Society*, 344(4), 1000–1028.

Bruzual, G. & Charlot, S. (2003b). Stellar population synthesis at the resolution of 2003. *Monthly Notices of the Royal Astronomical Society*, 344(4), 1000–1028.

Bruzual A., G. (1981). The spectrum of the extragalactic background light. *Revista Mexicana de Astronomia y Astrofisica, vol. 6*, 6, 19–21.

Bruzual A., G. (1983a). Spectral evolution of galaxies. I - Early-type systems. *The Astrophysical Journal*, 273, 105.

Bruzual A., G. (1983b). Spectral evolution of galaxies. I - Early-type systems. *The Astrophysical Journal*, 273, 105.

Bryant, J. J., Owers, M. S., Robotham, A. S. G., Croom, S. M., Driver, S. P., Drinkwater, M. J., Lorente, N. P. F., Cortese, L., Scott, N., Colless, M., Schaefer, A., Taylor, E. N., Konstantopoulos, I. S., Allen, J. T., Baldry, I., Barnes, L., Bauer, A. E., Bland-Hawthorn, J., Bloom, J. V., Brooks, A. M., Brough, S., Cecil, G., Couch, W., Croton, D., Davies, R., Ellis, S., Fogarty, L. M. R., Foster, C., Glazebrook, K., Goodwin, M., Green, A., Gunawardhana, M. L., Hampton, E., Ho, I.-T., Hopkins, A. M., Kewley, L., Lawrence, J. S., Leon-Saval, S. G., Leslie, S., McElroy, R., Lewis, G., Liske, J., López-Sánchez, A. R., Mahajan, S., Medling, A. M., Metcalfe, N., Meyer, M., Mould, J., Obreschkow, D., O'Toole, S., Pracy, M., Richards, S. N., Shanks, T., Sharp, R., Sweet, S. M., Thomas, A. D., Tonini, C., & Walcher, C. J. (2015). The SAMI Galaxy Survey: Instrument specification and target selection. *Monthly Notices of the Royal Astronomical Society*, 447(3), 2857–2879.

Bundy, K., Bershady, M. A., Law, D. R., Yan, R., Drory, N., MacDonald, N., Wake, D. A., Cherinka, B., Sánchez-Gallego, J. R., Weijmans, A.-M., Thomas, D., Tremonti, C., Masters, K., Coccato, L., Diamond-Stanic, A. M., Aragón-Salamanca, A., Avila-Reese, V., Badenes, C., Falcón-Barroso, J., Belfiore, F., Bizyaev, D., Blanc, G. A., Bland-Hawthorn,

J., Blanton, M. R., Brownstein, J. R., Byler, N., Cappellari, M., Conroy, C., Dutton, A. A., Emsellem, E., Etherington, J., Frinchaboy, P. M., Fu, H., Gunn, J. E., Harding, P., Johnston, E. J., Kauffmann, G., Kinemuchi, K., Klaene, M. A., Knapen, J. H., Leauthaud, A., Li, C., Lin, L., Maiolino, R., Malanushenko, V., Malanushenko, E., Mao, S., Maraston, C., McDermid, R. M., Merrifield, M. R., Nichol, R. C., Oravetz, D., Pan, K., Parejko, J. K., Sanchez, S. F., Schlegel, D., Simmons, A., Steele, O., Steinmetz, M., Thanjavur, K., Thompson, B. A., Tinker, J. L., van den Bosch, R. C. E., Westfall, K. B., Wilkinson, D., Wright, S., Xiao, T., & Zhang, K. (2014). OVERVIEW OF THE SDSS-IV MaNGA SURVEY: MAPPING NEARBY GALAXIES AT APACHE POINT OBSERVATORY. *The Astrophysical Journal*, 798(1), 7.

Burgarella, D., Buat, V., Gruppioni, C., Cucciati, O., Heinis, S., Berta, S., Béthermin, M., Bock, J., Cooray, A., Dunlop, J. S., Farrah, D., Franceschini, A., Le Floc'h, E., Lutz, D., Magnelli, B., Nordon, R., Oliver, S. J., Page, M. J., Popesso, P., Pozzi, F., Riguccini, L., Vaccari, M., & Viero, M. (2013). *Herschel* PEP/HerMES: The redshift evolution ($0 \leq z \leq 4$) of dust attenuation and of the total (UV+IR) star formation rate density. *Astronomy & Astrophysics*, 554, A70.

Calzetti, D., Kennicutt, R. C., Engelbracht, C. W., Leitherer, C., Draine, B. T., Kewley, L., Moustakas, J., Sosey, M., Dale, D. A., Gordon, K. D., & others (2007). The calibration of mid-infrared star formation rate indicators. *The Astrophysical Journal*, 666(2), 870.

Chabrier, G. (2003). Galactic Stellar and Substellar Initial Mass Function. *Publications of the Astronomical Society of the Pacific*, 115, 763–795.

Chen, Y.-M., Kauffmann, G., Tremonti, C. A., White, S., Heckman, T. M., Kovač, K., Bundy, K., Chisholm, J., Maraston, C., Schneider, D. P., Bolton, A. S., Weaver, B. A., & Brinkmann, J. (2012). Evolution of the most massive galaxies to z= 0.6 - I. A new method for physical parameter estimation. *Monthly Notices of the Royal Astronomical Society*, 421, 314–332.

Clerke, A. M. (2010). *A Popular History of Astronomy During the Nineteenth Century*.

Coelho, P., Barbuy, B., Meléndez, J., Schiavon, R. P., & Castilho, B. V. (2005). A library of high resolution synthetic stellar spectra from 300 nm to 1.8 μm with solar and α-enhanced composition. *Astronomy & Astrophysics*, 443, 735–746.

Colless, M. et al. (2001). The 2dF Galaxy Redshift Survey: spectra and redshifts. *Monthly Notices of the Royal Astronomical Society*, 328, 1039–1063.

Conroy, C. (2013). Modeling the panchromatic spectral energy distributions of galaxies. *arXiv preprint arXiv:1301.7095*.

Cooper, M. C., Newman, J. A., Madgwick, D. S., Gerke, B. F., Yan, R., & Davis, M. (2005). Measuring galaxy environments with deep redshift surveys. *The Astrophysical Journal*, 634(2), 833.

Crain, R. A., Schaye, J., Bower, R. G., Furlong, M., Schaller, M., Theuns, T., Dalla Vecchia, C., Frenk, C. S., McCarthy, I. G., Helly, J. C., Jenkins, A., Rosas-Guevara, Y. M., White, S. D. M., & Trayford, J. W. (2015). The EAGLE simulations of galaxy formation: calibration of subgrid physics and model variations. *Monthly Notices of the Royal Astronomical Society*, 450, 1937–1961.

Creasey, P., Theuns, T., & Bower, R. G. (2013). How supernova explosions power galactic winds. *Monthly Notices of the Royal Astronomical Society*, 429, 1922–1948.

da Cunha, E., Charlot, S., & Elbaz, D. (2008). A simple model to interpret the ultraviolet, optical and infrared emission from galaxies. *Monthly Notices of the Royal Astronomical Society*, 388(4), 1595–1617.

Davé, R., Thompson, R., & Hopkins, P. F. (2016). MUFASA: galaxy formation simulations with meshless hydrodynamics. *Monthly Notices of the Royal Astronomical Society*, 462, 3265–3284.

Davis, M., Efstathiou, G., Frenk, C. S., & White, S. D. M. (1985). The evolution of large-scale structure in a universe dominated by cold dark matter. *The Astrophysical Journal*, 292, 371–394.

Draine, B. T. & Li, A. (2007). Infrared Emission from Interstellar Dust. IV. The Silicate-Graphite-PAH Model in the Post-Spitzer Era. *The Astrophysical Journal*, 657, 810–837.

Dressler, A. (1980). Galaxy morphology in rich clusters - Implications for the formation and evolution of galaxies. *The Astrophysical Journal*, 236, 351.

Dressler, A. & Gunn, J. E. (1983). Spectroscopy of galaxies in distant clusters. II. The population of the 3C 295 cluster. *The Astrophysical Journal*, 270, 7–19.

Drory, N., Bender, R., & Hopp, U. (2004). Comparing Spectroscopic and Photometric Stellar Mass Estimates. *The Astrophysical Journal*, 616, L103–L106.

Drory, N., MacDonald, N., Bershady, M. A., Bundy, K., Gunn, J., Law, D. R., Smith, M., Stoll, R., Tremonti, C. A., Wake, D. A., Yan, R., Weijmans, A. M., Byler, N., Cherinka, B., Cope, F., Eigenbrot, A., Harding, P., Holder, D., Huehnerhoff, J., Jaehnig, K., Jansen, T. C., Klaene, M., Paat, A. M., Percival, J., & Sayres, C. (2015). THE MANGA INTE-GRAL FIELD UNIT FIBER FEED SYSTEM FOR THE SLOAN 2.5 M TELESCOPE. *The Astronomical Journal*, 149(2), 77.

D'Souza, R., Vegetti, S., & Kauffmann, G. (2015). The massive end of the stellar mass function. *Monthly Notices of the Royal Astronomical Society*, 454, 4027–4036.

Efstathiou, G., Ellis, R. S., & Peterson, B. A. (1988). Analysis of a complete galaxy redshift survey. II - The field-galaxy luminosity function. *Monthly Notices of the Royal Astronomical Society*, 232, 431–461.

Eggen, O. J., Lynden-Bell, D., & Sandage, A. R. (1962). Evidence from the motions of old stars that the Galaxy collapsed. *The Astrophysical Journal*, 136, 748.

Eisenstein, D. J., Weinberg, D. H., Agol, E., Aihara, H., Allende Prieto, C., Anderson, S. F., Arns, J. A., Aubourg, É., Bailey, S., Balbinot, E., & et al. (2011). SDSS-III: Massive Spectroscopic Surveys of the Distant Universe, the Milky Way, and Extra-Solar Planetary Systems. *The Astronomical Journal*, 142, 72.

Elbaz, D., Daddi, E., Le Borgne, D., Dickinson, M., Alexander, D. M., Chary, R. R., Starck, J. L., Brand t, W. N., Kitzbichler, M., MacDonald, E., Nonino, M., Popesso, P., Stern, D., & Vanzella, E. (2007). The reversal of the star formation-density relation in the distant universe. *Astronomy & Astrophysics*, 468, 33–48.

Faber, S. M. (1972). Quadratic programming applied to the problem of galaxy population synthesis. *Astronomy & Astrophysics*, 20, 361–374.

Ferland, G. J., Porter, R. L., van Hoof, P. A. M., Williams, R. J. R., Abel, N. P., Lykins, M. L., Shaw, G., Henney, W. J., & Stancil, P. C. (2013). The 2013 Release of Cloudy. *Revista Mexicana de Astronomía y Astrofísica*, 49, 137–163.

Freeman, K. C. (1970). On the Disks of Spiral and so Galaxies. *The Astrophysical Journal*, 160, 811.

Gallazzi, A., Charlot, S., Brinchmann, J., White, S. D. M., & Tremonti, C. A. (2005). The ages and metallicities of galaxies in the local universe. *Monthly Notices of the Royal Astronomical Society*, 362, 41–58.

Geha, M., Blanton, M. R., Yan, R., & Tinker, J. L. (2012). A Stellar Mass Threshold for Quenching of Field Galaxies. *The Astrophysical Journal*, 757, 85.

Graham, A. W. & Driver, S. P. (2005). A Concise Reference to (Projected) Sérsic $R^{1/n}$ Quantities, Including Concentration, Profile Slopes, Petrosian Indices, and Kron Magnitudes. *Publications of the Astronomical Society of Australia*, 22, 118–127.

Gunn, J. E., Siegmund, W. A., Mannery, E. J., Owen, R. E., Hull, C. L., Leger, R. F., Carey, L. N., Knapp, G. R., York, D. G., Boroski, W. N., Kent, S. M., Lupton, R. H., Rockosi, C. M., Evans, M. L., Waddell, P., Anderson, J. E., Annis, J., Barentine, J. C., Bartoszek, L. M., Bastian, S., Bracker, S. B., Brewington, H. J., Briegel, C. I., Brinkmann, J., Brown, Y. J., Carr, M. A., Czarapata, P. C., Drennan, C. C., Dombeck, T., Federwitz, G. R., Gillespie, B. A., Gonzales, C., Hansen, S. U., Harvanek, M., Hayes, J., Jordan, W., Kinney, E., Klaene, M., Kleinman, S. J., Kron, R. G., Kresinski, J., Lee, G., Limmongkol, S., Lindenmeyer, C. W., Long, D. C., Loomis, C. L., McGehee, P. M., Mantsch, P. M., Neilsen, Eric H., J., Neswold, R. M., Newman, P. R., Nitta, A., Peoples, John, J., Pier, J. R., Prieto, P. S., Prosapio, A., Rivetta, C., Schneider, D. P., Snedden, S., & Wang, S.-i. (2006). The 2.5 m Telescope of the Sloan Digital Sky Survey. *The Astronomical Journal*, 131, 2332–2359.

Guth, A. H. (1981). Inflationary universe: A possible solution to the horizon and flatness problems. *Phys. Rev. D*, 23, 347–356.

Hahn, C., Blanton, M. R., Moustakas, J., Coil, A. L., Cool, R. J., Eisenstein, D. J., Skibba, R. A., Wong, K. C., & Zhu, G. (2015). PRIMUS: EFFECTS OF GALAXY ENVIRONMENT ON THE QUIESCENT FRACTION EVOLUTION AT z < 0.8. *The Astrophysical Journal*, 806(2), 162.

Hamilton, D. (1985). The spectral evolution of galaxies. I. an observational approach. *The Astrophysical Journal*, 297, 371–389.

Hopkins, P. F., Quataert, E., & Murray, N. (2012). Stellar feedback in galaxies and the origin of galaxy-scale winds. *Monthly Notices of the Royal Astronomical Society*, 421, 3522–3537.

Hubble, E. (1929). A Relation between Distance and Radial Velocity among Extra-Galactic Nebulae. *Proceedings of the National Academy of Science*, 15, 168–173.

Hubble, E. & Humason, M. L. (1931). The Velocity-Distance Relation among Extra-Galactic Nebulae. *The Astrophysical Journal*, 74, 43.

Huchra, J. P., Geller, M. J., & Corwin, Jr., H. G. (1995). The CfA redshift survey: Data for the NGP +36 zone. *The Astrophysical Journal, Supplement*, 99, 391–403.

Ilbert, O., McCracken, H. J., Le Fèvre, O., Capak, P., Dunlop, J., Karim, A., Renzini, M. A., Caputi, K., Boissier, S., Arnouts, S., Aussel, H., Comparat, J., Guo, Q., Hudelot, P., Kartaltepe, J., Kneib, J. P., Krogager, J. K., Le Floc'h, E., Lilly, S., Mellier, Y., Milvang-Jensen, B., Moutard, T., Onodera, M., Richard, J., Salvato, M., Sanders, D. B., Scoville, N., Silverman, J. D., Taniguchi, Y., Tasca, L., Thomas, R., Toft, S., Tresse, L., Vergani, D., Wolk, M., & Zirm, A. (2013). Mass assembly in quiescent and star-forming galaxies since z ≳ 4 from UltraVISTA. *Astronomy & Astrophysics*, 556, A55.

Karim, A., Schinnerer, E., Martínez-Sansigre, A., Sargent, M. T., van der Wel, A., Rix, H.-W., Ilbert, O., Smolčić, V., Carilli, C., Pannella, M., Koekemoer, A. M., Bell, E. F., & Salvato, M. (2011). THE STAR FORMATION HISTORY OF MASS-SELECTED GALAXIES IN THE COSMOS FIELD. *The Astrophysical Journal*, 730(2), 61.

Kauffmann, G., Heckman, T. M., Simon White, D. M., Charlot, S., Tremonti, C., Brinchmann, J., Bruzual, G., Peng, E. W., Seibert, M., Bernardi, M., Blanton, M., Brinkmann, J., Castander, F., Csábai, I., Fukugita, M., Ivezic, Z., Munn, J. A., Nichol, R. C., Padmanabhan, N., Thakar, A. R., Weinberg, D. H., & York, D. (2003). Stellar masses and star formation histories for 10^5 galaxies from the Sloan Digital Sky Survey. *Monthly Notices of the Royal Astronomical Society*, 341(1), 33–53.

Kauffmann, G., Li, C., Zhang, W., & Weinmann, S. (2013). A re-examination of galactic conformity and a comparison with semi-analytic models of galaxy formation. *Monthly Notices of the Royal Astronomical Society*, 430, 1447–1456.

Kauffmann, G., White, S. D. M., Heckman, T. M., Ménard, B., Brinchmann, J., Charlot, S., Tremonti, C., & Brinkmann, J. (2004). The environmental dependence of the relations between stellar mass, structure, star formation and nuclear activity in galaxies: Galaxy structure, star formation and nuclear activity. *Monthly Notices of the Royal Astronomical Society*, 353(3), 713–731.

Kennicutt, R. C. & Evans, N. J. (2012). Star Formation in the Milky Way and Nearby Galaxies. *Annual Review of Astronomy and Astrophysics*, 50(1), 531–608.

Kennicutt, Jr., R. C. (1998). The Global Schmidt Law in Star-forming Galaxies. *The Astrophysical Journal*, 498, 541–552.

Kennicutt, Jr., R. C., Tamblyn, P., & Congdon, C. E. (1994). Past and future star formation in disk galaxies. *The Astrophysical Journal*, 435, 22–36.

Kewley, L. J. & Ellison, S. L. (2008). Metallicity Calibrations and the Mass-Metallicity Relation for Star-forming Galaxies. *The Astrophysical Journal*, 681, 1183–1204.

Kewley, L. J., Groves, B., Kauffmann, G., & Heckman, T. (2006). The host galaxies and classification of active galactic nuclei. *Monthly Notices of the Royal Astronomical Society*, 372, 961–976.

Kroupa, P. (2001). On the variation of the initial mass function. *Monthly Notices of the Royal Astronomical Society*, 322, 231–246.

Law, D. R., Cherinka, B., Yan, R., Andrews, B. H., Bershady, M. A., Bizyaev, D., Blanc, G. A., Blanton, M. R., Bolton, A. S., Brownstein, J. R., Bundy, K., Chen, Y., Drory, N., D'Souza, R., Fu, H., Jones, A., Kauffmann, G., MacDonald, N., Masters, K. L., New-man, J. A., Parejko, J. K., Sánchez-Gallego, J. R., Sánchez, S. F., Schlegel, D. J., Thomas, D., Wake, D. A., Weijmans, A.-M., Westfall, K. B., & Zhang, K. (2016). THE DATA RE-DUCTION PIPELINE FOR THE SDSS-IV MaNGA IFU GALAXY SURVEY. *The Astronomical Journal*, 152(4), 83.

Le Borgne, J. F., Bruzual, G., Pelló, R., Lançon, A., Rocca-Volmerange, B., Sanahuja, B., Schaerer, D., Soubiran, C., & Vílchez-Gómez, R. (2003). STELIB: A library of stellar spectra at R ~2000. *Astronomy & Astrophysics*, 402, 433–442.

Lee, J. C., Gil de Paz, A., Tremonti, C., Kennicutt, R. C., Salim, S., Bothwell, M., Calzetti, D., Dalcanton, J., Dale, D., Engelbracht, C., José G. Funes, S. J., Johnson, B., Sakai, S., Skillman, E., van Zee, L., Walter, F., & Weisz, D. (2009). COMPARISON OF Hα AND UV STAR FORMATION RATES IN THE LOCAL VOLUME: SYSTEMATIC DIS-CREPANCIES FOR DWARF GALAXIES. *The Astrophysical Journal*, 706(1), 599–613.

Leitherer, C. & Heckman, T. M. (1995). Synthetic properties of starburst galaxies. *The Astrophysical Journal, Supplement*, 96, 9–38.

Leja, J., Johnson, B. D., Conroy, C., van Dokkum, P. G., & Byler, N. (2017). Deriving Physical Properties from Broadband Photometry with Prospector: Description of the Model and a Demonstration of its Accuracy Using 129 Galaxies in the Local Universe. *The Astrophysical Journal*, 837, 170.

Lewis, I., Balogh, M., De Propris, R., Couch, W., Bower, R., Offer, A., Bland-Hawthorn, J., Baldry, I. K., Baugh, C., Bridges, T., Cannon, R., Cole, S., Colless, M., Collins, C., Cross, N., Dalton, G., Driver, S. P., Efstathiou, G., Ellis, R. S., Frenk, C. S., Glazebrook, K., Hawkins, E., Jackson, C., Lahav, O., Lumsden, S., Maddox, S., Madgwick, D., Nor-berg, P., Peacock, J. A., Percival, W., Peterson, B. A., Sutherland, W., & Taylor, K. (2002).

The 2dF Galaxy Redshift Survey: the environmental dependence of galaxy star formation rates near clusters. *Monthly Notices of the Royal Astronomical Society*, 334, 673–683.

Li, C. & White, S. D. M. (2009). The distribution of stellar mass in the low-redshift Universe. *Monthly Notices of the Royal Astronomical Society*, 398, 2177–2187.

Lynn, W. T. (1901). Democritus and Galileo on the Milky Way. *The Observatory*, 24, 382–383.

Madau, P. & Dickinson, M. (2014). Cosmic Star-Formation History. *Annual Review of Astronomy and Astrophysics*, 52(1), 415–486.

Madau, P., Pozzetti, L., & Dickinson, M. (1998). The Star Formation History of Field Galaxies. *The Astrophysical Journal*, 498, 106–116.

Martin, D. C., Fanson, J., Schiminovich, D., Morrissey, P., Friedman, P. G., Barlow, T. A., Conrow, T., Grange, R., Jelinsky, P. N., Milliard, B., Siegmund, O. H. W., Bianchi, L., Byun, Y.-I., Donas, J., Forster, K., Heckman, T. M., Lee, Y.-W., Madore, B. F., Malina, R. F., Neff, S. G., Rich, R. M., Small, T., Surber, F., Szalay, A. S., Welsh, B., & Wyder, T. K. (2005). The Galaxy Evolution Explorer: A Space Ultraviolet Survey Mission. *The Astrophysical Journal*, 619(1), L1–L6.

Moustakas, J., Coil, A. L., Aird, J., Blanton, M. R., Cool, R. J., Eisenstein, D. J., Mendez, A. J., Wong, K. C., Zhu, G., & Arnouts, S. (2013a). PRIMUS: CONSTRAINTS ON STAR FORMATION QUENCHING AND GALAXY MERGING, AND THE EVOLUTION OF THE STELLAR MASS FUNCTION FROM $z = 0$-1. *The Astrophysical Journal*, 767(1), 50.

Moustakas, J., Coil, A. L., Aird, J., Blanton, M. R., Cool, R. J., Eisenstein, D. J., Mendez, A. J., Wong, K. C., Zhu, G., & Arnouts, S. (2013b). PRIMUS: CONSTRAINTS ON STAR FORMATION QUENCHING AND GALAXY MERGING, AND THE EVOLUTION OF THE STELLAR MASS FUNCTION FROM $z = 0$-1. *The Astrophysical Journal*, 767(1), 50.

Muzzin, A., Marchesini, D., Stefanon, M., Franx, M., McCracken, H. J., Milvang-Jensen, B., Dunlop, J. S., Fynbo, J. P. U., Brammer, G., Labbé, I., & van Dokkum, P. G. (2013). THE EVOLUTION OF THE STELLAR MASS FUNCTIONS OF STAR-FORMING AND QUIESCENT GALAXIES TO $z = 4$ FROM THE COSMOS/UltraVISTA SURVEY. *The Astrophysical Journal*, 777(1), 18.

Muzzin, A., Marchesini, D., van Dokkum, P. G., Labbé, I., Kriek, M., & Franx, M. (2009). A Near-Infrared Spectroscopic Survey of K-Selected Galaxies at z~2.3: Comparison of Stellar Population Synthesis Codes and Constraints from the Rest-Frame NIR. *The Astrophysical Journal*, 701, 1839–1864.

Noeske, K. G., Weiner, B. J., Faber, S. M., Papovich, C., Koo, D. C., Somerville, R. S., Bundy, K., Conselice, C. J., Newman, J. A., Schiminovich, D., Le Floc'h, E., Coil, A. L., Rieke, G. H., Lotz, J. M., Primack, J. R., Barmby, P., Cooper, M. C., Davis, M., Ellis, R. S., Fazio, G. G., Guhathakurta, P., Huang, J., Kassin, S. A., Martin, D. C., Phillips, A. C., Rich, R. M., Small, T. A., Willmer, C. N. A., & Wilson, G. (2007). Star Formation in AEGIS Field Galaxies since z=1.1: The Dominance of Gradually Declining Star Formation, and the Main Sequence of Star-forming Galaxies. *The Astrophysical Journal, Letters*, 660, L43–L46.

Noll, S., Burgarella, D., Giovannoli, E., Buat, V., Marcillac, D., & Muñoz-Mateos, J. C. (2009). Analysis of galaxy spectral energy distributions from far-UV to far-IR with CIGALE: studying a SINGS test sample. *Astronomy & Astrophysics*, 507, 1793–1813.

Norberg, P., Baugh, C. M., Hawkins, E., Maddox, S., Madgwick, D., Lahav, O., Cole, S., Frenk, C. S., Baldry, I., Bland-Hawthorn, J., Bridges, T., Cannon, R., Colless, M., Collins, C., Couch, W., Dalton, G., De Propris, R., Driver, S. P., Efstathiou, G., Ellis, R. S., Glazebrook, K., Jackson, C., Lewis, I., Lumsden, S., Peacock, J. A., Peterson, B. A., Sutherland, W., & Taylor, K. (2002). The 2dF Galaxy Redshift Survey: the dependence of galaxy clustering on luminosity and spectral type. *Monthly Notices of the Royal Astronomical Society*, 332, 827–838.

Overzier, R. A., Heckman, T. M., Wang, J., Armus, L., Buat, V., Howell, J., Meurer, G., Seibert, M., Siana, B., Basu-Zych, A., Charlot, S., Gonçalves, T. S., Martin, D. C., Neill, J. D., Rich, R. M., Salim, S., & Schiminovich, D. (2011). Dust Attenuation in UV-selected Starbursts at High Redshift and Their Local Counterparts: Implications for the Cosmic Star Formation Rate Density. *The Astrophysical Journal*, 726, L7.

Papovich, C., Dickinson, M., & Ferguson, H. C. (2001). The Stellar Populations and Evolution of Lyman Break Galaxies. *The Astrophysical Journal*, 559, 620–653.

Park, C., Choi, Y.-Y., Vogeley, M. S., Gott, J. Richard, I., Blanton, M. R., & SDSS Collaboration (2007). Environmental Dependence of Properties of Galaxies in the Sloan Digital Sky Survey. *The Astrophysical Journal*, 658, 898–916.

Peebles, P. J. E. (1982). Large-scale background temperature and mass fluctuations due to scale-invariant primeval perturbations. *The Astrophysical Journal*, 263, L1.

Peng, Y.-j., Lilly, S. J., Kovač, K., Bolzonella, M., Pozzetti, L., Renzini, A., Zamorani, G., Ilbert, O., Knobel, C., Iovino, A., Maier, C., Cucciati, O., Tasca, L., Carollo, C. M., Silverman, J., Kampczyk, P., de Ravel, L., Sanders, D., Scoville, N., Contini, T., Mainieri, V., Scodeggio, M., Kneib, J.-P., Le Fèvre, O., Bardelli, S., Bongiorno, A., Caputi, K., Coppa, G., de la Torre, S., Franzetti, P., Garilli, B., Lamareille, F., Le Borgne, J.-F., Le Brun, V., Mignoli, M., Montero, E. P., Pello, R., Ricciardelli, E., Tanaka, M., Tresse, L., Vergani, D., Welikala, N., Zucca, E., Oesch, P., Abbas, U., Barnes, L., Bordoloi, R., Bottini, D., Cappi, A., Cassata, P., Cimatti, A., Fumana, M., Hasinger, G., Koekemoer, A., Leauthaud, A., Maccagni, D., Marinoni, C., McCracken, H., Memeo, P., Meneux, B., Nair, P., Porciani, C., Presotto, V., & Scaramella, R. (2010). MASS AND ENVIRONMENT AS DRIVERS OF GALAXY EVOLUTION IN SDSS AND zCOSMOS AND THE ORIGIN OF THE SCHECHTER FUNCTION. *The Astrophysical Journal*, 721(1), 193–221.

Peng, Y.-j., Lilly, S. J., Renzini, A., & Carollo, M. (2012). MASS AND ENVIRONMENT AS DRIVERS OF GALAXY EVOLUTION. II. THE QUENCHING OF SATELLITE GALAXIES AS THE ORIGIN OF ENVIRONMENTAL EFFECTS. *The Astrophysical Journal*, 757(1), 4.

Penzias, A. A. & Wilson, R. W. (1965). A Measurement of Excess Antenna Temperature at 4080 Mc/s. *The Astrophysical Journal*, 142, 419–421.

Prugniel, P. & Soubiran, C. (2004). New release of the ELODIE library. *arXiv Astrophysics e-prints*.

Riess, A. G. et al. (1998). Observational evidence from supernovae for an accelerating universe and a cosmological constant. *Astron. J.*, 116, 1009–1038.

Roberts, M. S. & Haynes, M. P. (1994). Physical Parameters along the Hubble Sequence. *Annual Review of Astronomy and Astrophysics*, 32, 115–152.

Rubin, V. C., Thonnard, N., & Ford, Jr., W. K. (1980). Rotational properties of 21 SC galaxies with a large range of luminosities and radii, from NGC 4605 /R = 4kpc/ to UGC 2885 /R = 122 kpc/. *The Astrophysical Journal*, 238, 471.

Salim, S., Rich, R. M., Charlot, S., Brinchmann, J., Johnson, B. D., Schiminovich, D., Seibert, M., Mallery, R., Heckman, T. M., Forster, K., & others (2007a). UV Star Formation Rates in the Local Universe. *The Astrophysical Journal Supplement Series*, 173(2), 267.

Salim, S., Rich, R. M., Charlot, S., Brinchmann, J., Johnson, B. D., Schiminovich, D., Seibert, M., Mallery, R., Heckman, T. M., Forster, K., & others (2007b). UV Star Formation Rates in the Local Universe. *The Astrophysical Journal Supplement Series*, 173(2), 267.

Salpeter, E. E. (1955). The Luminosity Function and Stellar Evolution. *The Astrophysical Journal*, 121, 161.

Sánchez, S. F., Kennicutt, R. C., Gil de Paz, A., van de Ven, G., Vílchez, J. M., Wisotzki, L., Walcher, C. J., Mast, D., Aguerri, J. A. L., Albiol-Pérez, S., Alonso-Herrero, A., Alves, J., Bakos, J., Bartáková, T., Bland-Hawthorn, J., Boselli, A., Bomans, D. J., Castillo-Morales, A., Cortijo-Ferrero, C., de Lorenzo-Cáceres, A., del Olmo, A., Dettmar, R.-J., Díaz, A., Ellis, S., Falcón-Barroso, J., Flores, H., Gallazzi, A., García-Lorenzo, B., González Delgado, R., Gruel, N., Haines, T., Hao, C., Husemann, B., Iglésias-Páramo, J., Jahnke, K., Johnson, B., Jungwiert, B., Kalinova, V., Kehrig, C., Kupko, D., López-Sánchez, A. R., Lyubenova, M., Marino, R. A., Mármol-Queraltó, E., Márquez, I., Masegosa, J., Meidt, S., Mendez-Abreu, J., Monreal-Ibero, A., Montijo, C., Mourão, A. M., Palacios-Navarro, G., Papaderos, P., Pasquali, A., Peletier, R., Pérez, E., Pérez, I., Quirrenbach, A., Relaño, M., Rosales-Ortega, F. F., Roth, M. M., Ruiz-Lara, T., Sánchez-Blázquez, P., Sengupta, C., Singh, R., Stanishev, V., Trager, S. C., Vazdekis, A., Viironen, K., Wild, V., Zibetti, S., & Ziegler, B. (2012). CALIFA, the Calar Alto Legacy Integral Field Area survey: I. Survey presentation⋆. *Astronomy & Astrophysics*, 538, A8.

Sánchez-Blázquez, P., Peletier, R. F., Jiménez-Vicente, J., Cardiel, N., Cenarro, A. J., Falcón-Barroso, J., Gorgas, J., Selam, S., & Vazdekis, A. (2006). Medium-resolution Isaac Newton Telescope library of empirical spectra. *Monthly Notices of the Royal Astronomical Society*, 371, 703–718.

Schmidt, M. (1959). The Rate of Star Formation. *The Astrophysical Journal*, 129, 243.

Schreiber, C., Pannella, M., Elbaz, D., Béthermin, M., Inami, H., Dickinson, M., Magnelli, B., Wang, T., Aussel, H., Daddi, E., Juneau, S., Shu, X., Sargent, M. T., Buat, V., Faber, S. M., Ferguson, H. C., Giavalisco, M., Koekemoer, A. M., Magdis, G., Morrison, G. E., Papovich, C., Santini, P., & Scott, D. (2015). The Herschel view of the dominant mode of galaxy growth from z = 4 to the present day. *Astronomy & Astrophysics*, 575, A74.

Schulz, J., Fritze-v. Alvensleben, U., Möller, C. S., & Fricke, K. J. (2002). Spectral and photometric evolution of simple stellar populations at various metallicities. *Astronomy & Astrophysics*, 392, 1–11.

Shectman, S. A., Landy, S. D., Oemler, A., Tucker, D. L., Lin, H., Kirshner, R. P., & Schechter, P. L. (1996). The Las Campanas Redshift Survey. *The Astrophysical Journal*, 470, 172–188.

Sijacki, D., Vogelsberger, M., Genel, S., Springel, V., Torrey, P., Snyder, G. F., Nelson, D., & Hernquist, L. (2015). The Illustris simulation: the evolving population of black holes across cosmic time. *Monthly Notices of the Royal Astronomical Society*, 452, 575–596.

Smee, S. A., Gunn, J. E., Uomoto, A., Roe, N., Schlegel, D., Rockosi, C. M., Carr, M. A., Leger, F., Dawson, K. S., Olmstead, M. D., Brinkmann, J., Owen, R., Barkhouser, R. H., Honscheid, K., Harding, P., Long, D., Lupton, R. H., Loomis, C., Anderson, L., Annis, J., Bernardi, M., Bhardwaj, V., Bizyaev, D., Bolton, A. S., Brewington, H., Briggs, J. W., Burles, S., Burns, J. G., Castander, F. J., Connolly, A., Davenport, J. R. A., Ebelke, G., Epps, H., Feldman, P. D., Friedman, S. D., Frieman, J., Heckman, T., Hull, C. L., Knapp, G. R., Lawrence, D. M., Loveday, J., Mannery, E. J., Malanushenko, E., Malanushenko, V., Merrelli, A. J., Muna, D., Newman, P. R., Nichol, R. C., Oravetz, D., Pan, K., Pope, A. C., Ricketts, P. G., Shelden, A., Sandford, D., Siegmund, W., Simmons, A., Smith, D. S., Snedden, S., Schneider, D. P., SubbaRao, M., Tremonti, C., Waddell, P., & York, D. G. (2013). THE MULTI-OBJECT, FIBER-FED SPECTROGRAPHS FOR THE SLOAN DIGITAL SKY SURVEY AND THE BARYON OSCILLATION SPECTRO-SCOPIC SURVEY. *The Astronomical Journal*, 146(2), 32.

Smoot, G. F., Bennett, C. L., Kogut, A., Wright, E. L., Aymon, J., Boggess, N. W., Cheng, E. S., de Amici, G., Gulkis, S., Hauser, M. G., Hinshaw, G., Jackson, P. D., Janssen, M., Kaita, E., Kelsall, T., Keegstra, P., Lineweaver, C., Loewenstein, K., Lubin, P., Mather, J., Meyer, S. S., Moseley, S. H., Murdock, T., Rokke, L., Silverberg, R. F., Tenorio, L., Weiss, R., & Wilkinson, D. T. (1992). Structure in the COBE Differential Microwave Radiometer First-Year Maps. *The Astrophysical Journal*, 396, L1.

Somerville, R. S. & Davé, R. (2015). Physical Models of Galaxy Formation in a Cosmological Framework. *Annual Review of Astronomy and Astrophysics*, 53, 51–113.

Speagle, J. S., Steinhardt, C. L., Capak, P. L., & Silverman, J. D. (2014). A Highly Consistent Framework for the Evolution of the Star-Forming "Main Sequence" from z ~0-6. *The Astrophysical Journal Supplement Series*, 214, 15.

Spinrad, H. & Taylor, B. J. (1971). The Stellar Content of the Nuclei of Nearby Galaxies. I. M31, M32, and M81. *The Astrophysical Journal, Supplement*, 22, 445.

Strateva, I., Ivezić, Ž., Knapp, G. R., Narayanan, V. K., Strauss, M. A., Gunn, J. E., Lupton, R. H., Schlegel, D., Bahcall, N. A., Brinkmann, J., Brunner, R. J., Budavári, T.,

Csabai, I., Castander, F. J., Doi, M., Fukugita, M., Győry, Z., Hamabe, M., Hennessy, G., Ichikawa, T., Kunszt, P. Z., Lamb, D. Q., McKay, T. A., Okamura, S., Racusin, J., Sekiguchi, M., Schneider, D. P., Shimasaku, K., & York, D. (2001). Color Separation of Galaxy Types in the Sloan Digital Sky Survey Imaging Data. *The Astronomical Journal*, 122, 1861–1874.

Strauss, M. A., Weinberg, D. H., Lupton, R. H., Narayanan, V. K., Annis, J., Bernardi, M., Blanton, M., Burles, S., Connolly, A. J., Dalcanton, J., Doi, M., Eisenstein, D., Frieman, J. A., Fukugita, M., Gunn, J. E., Ivezić, Ž., Kent, S., Kim, R. S. J., Knapp, G. R., Kron, R. G., Munn, J. A., Newberg, H. J., Nichol, R. C., Okamura, S., Quinn, T. R., Richmond, M. W., Schlegel, D. J., Shimasaku, K., SubbaRao, M., Szalay, A. S., Vanden Berk, D., Vogeley, M. S., Yanny, B., Yasuda, N., York, D. G., & Zehavi, I. (2002). Spectroscopic Target Selection in the Sloan Digital Sky Survey: The Main Galaxy Sample. *The Astronomical Journal*, 124, 1810–1824.

Tinker, J. L., Brownstein, J. R., Guo, H., Leauthaud, A., Maraston, C., Masters, K., Montero-Dorta, A. D., Thomas, D., Tojeiro, R., Weiner, B., Zehavi, I., & Olmstead, M. D. (2017). The Correlation between Halo Mass and Stellar Mass for the Most Massive Galaxies in the Universe. *The Astrophysical Journal*, 839(2), 121.

Tomczak, A. R., Quadri, R. F., Tran, K.-V. H., Labbé, I., Straatman, C. M. S., Papovich, C., Glazebrook, K., Allen, R., Brammer, G. B., Kacprzak, G. G., Kawinwanichakij, L., Kelson, D. D., McCarthy, P. J., Mehrtens, N., Monson, A. J., Persson, S. E., Spitler, L. R., Tilvi, V., & van Dokkum, P. (2014). GALAXY STELLAR MASS FUNCTIONS FROM ZFOURGE/CANDELS: AN EXCESS OF LOW-MASS GALAXIES SINCE $z = 2$ AND THE RAPID BUILDUP OF QUIESCENT GALAXIES. *The Astrophysical Journal*, 783(2), 85.

Tremonti, C. A., Heckman, T. M., Kauffmann, G., Brinchmann, J., Charlot, S., White, S. D. M., Seibert, M., Peng, E. W., Schlegel, D. J., Uomoto, A., Fukugita, M., & Brinkmann, J. (2004). The Origin of the Mass-Metallicity Relation: Insights from 53,000 Star-forming Galaxies in the Sloan Digital Sky Survey. *The Astrophysical Journal*, 613(2), 898–913.

Wake, D. A., Bundy, K., Diamond-Stanic, A. M., Yan, R., Blanton, M. R., Bershady, M. A., Sánchez-Gallego, J. R., Drory, N., Jones, A., Kauffmann, G., Law, D. R., Li, C., MacDonald, N., Masters, K., Thomas, D., Tinker, J., Weijmans, A.-M., & Brownstein, J. R. (2017). The SDSS-IV MaNGA Sample: Design, Optimization, and Usage Considerations. *The Astronomical Journal*, 154, 86.

Walcher, J., Groves, B., Budavári, T., & Dale, D. (2011). Fitting the integrated spectral energy distributions of galaxies. *Astrophysics and Space Science*, 331, 1–52.

Worthey, G. (1994). Comprehensive stellar population models and the disentanglement of age and metallicity effects. *The Astrophysical Journal Supplement Series*, 95, 107.

Worthey, G. & Ottaviani, D. L. (1997). Hγ and Hδ Absorption Features in Stars and Stellar Populations. *The Astrophysical Journal Supplement Series*, 111, 377–386.

Wright, E. L., Eisenhardt, P. R. M., Mainzer, A. K., Ressler, M. E., Cutri, R. M., Jarrett, T., Kirkpatrick, J. D., Padgett, D., McMillan, R. S., Skrutskie, M., Stanford, S. A., Cohen, M., Walker, R. G., Mather, J. C., Leisawitz, D., Gautier, T. N., McLean, I., Benford, D., Lonsdale, C. J., Blain, A., Mendez, B., Irace, W. R., Duval, V., Liu, F., Royer, D., Heinrichsen, I., Howard, J., Shannon, M., Kendall, M., Walsh, A. L., Larsen, M., Cardon, J. G., Schick, S., Schwalm, M., Abid, M., Fabinsky, B., Naes, L., & Tsai, C.-W. (2010). THE WIDE-FIELD INFRARED SURVEY EXPLORER (WISE): MISSION DESCRIPTION AND INITIAL ON-ORBIT PERFORMANCE. *The Astronomical Journal*, 140(6), 1868–1881.

Wyder, T. K., Martin, D. C., Schiminovich, D., Seibert, M., Budavári, T., Treyer, M. A., Barlow, T. A., Forster, K., Friedman, P. G., Morrissey, P., Neff, S. G., Small, T., Bianchi, L., Donas, J., Heckman, T. M., Lee, Y.-W., Madore, B. F., Milliard, B., Rich, R. M., Szalay, A. S., Welsh, B. Y., & Yi, S. K. (2007). The UV-Optical Galaxy Color-Magnitude Diagram. I. Basic Properties. *The Astrophysical Journal Supplement Series*, 173, 293–314.

Wyder, T. K., Martin, D. C., Schiminovich, D., Seibert, M., Budavari, T., Treyer, M. A., Barlow, T. A., Forster, K., Friedman, P. G., Morrissey, P., Neff, S. G., Small, T., Bianchi, L., Donas, J., Heckman, T. M., Lee, Y.-W., Madore, B. F., Milliard, B., Rich, R. M., Szalay, A. S., Welsh, B. Y., & Yi, S. K. (2007). The UV-Optical Galaxy Color-Magnitude Diagram. I. Basic Properties. *The Astrophysical Journal Supplement Series*, 173(2), 293–314.

Yan, R., Chen, Y., Lazarz, D., Bizyaev, D., Maraston, C., Stringfellow, G. S., McCarthy, K., Meneses-Goytia, S., Law, D. R., Thomas, D., Falcon Barroso, J., Sánchez-Gallego, J. R., Schlafly, E., Zheng, Z., Argudo-Fernández, M., Beaton, R. L., Beers, T. C., Bershady, M., Blanton, M. R., Brownstein, J., Bundy, K., Chambers, K. C., Cherinka, B., De Lee, N., Drory, N., Galbany, L., Holtzman, J., Imig, J., Kaiser, N., Kinemuchi, K., Liu, C., Luo, A.-L., Magnier, E., Majewski, S., Nair, P., Oravetz, A., Oravetz, D., Pan, K., Sobeck, J., Stassun, K., Talbot, M., Tremonti, C., Waters, C., Weijmans, A.-M., Wilhelm, R., Zasowski, G., Zhao, G., & Zhao, Y.-H. (2018). SDSS-IV MaStar – A Large and Comprehensive Empirical Stellar Spectral Library: First Release. *arXiv e-prints*, (pp. arXiv:1812.02745).

York, D. G., Adelman, J., Anderson, John E., J., Anderson, S. F., Annis, J., Bahcall, N. A., Bakken, J. A., Barkhouser, R., Bastian, S., Berman, E., Boroski, W. N., Bracker, S., Briegel,

C., Briggs, J. W., Brinkmann, J., Brunner, R., Burles, S., Carey, L., Carr, M. A., Castander, F. J., Chen, B., Colestock, P. L., Connolly, A. J., Crocker, J. H., Csabai, I., Czarapata, P. C., Davis, J. E., Doi, M., Dombeck, T., Eisenstein, D., Ellman, N., Elms, B. R., Evans, M. L., Fan, X., Federwitz, G. R., Fiscelli, L., Friedman, S., Frieman, J. A., Fukugita, M., Gillespie, B., Gunn, J. E., Gurbani, V. K., de Haas, E., Haldeman, M., Harris, F. H., Hayes, J., Heckman, T. M., Hennessy, G. S., Hindsley, R. B., Holm, S., Holmgren, D. J., Huang, C.-h., Hull, C., Husby, D., Ichikawa, S.-I., Ichikawa, T., Ivezić, Ž., Kent, S., Kim, R. S. J., Kinney, E., Klaene, M., Kleinman, A. N., Kleinman, S., Knapp, G. R., Korienek, J., Kron, R. G., Kunszt, P. Z., Lamb, D. Q., Lee, B., Leger, R. F., Limmongkol, S., Lindenmeyer, C., Long, D. C., Loomis, C., Loveday, J., Lucinio, R., Lupton, R. H., MacKinnon, B., Mannery, E. J., Mantsch, P. M., Margon, B., McGehee, P., McKay, T. A., Meiksin, A., Merelli, A., Monet, D. G., Munn, J. A., Narayanan, V. K., Nash, T., Neilsen, E., Neswold, R., Newberg, H. J., Nichol, R. C., Nicinski, T., Nonino, M., Okada, N., Okamura, S., Ostriker, J. P., Owen, R., Pauls, A. G., Peoples, J., Peterson, R. L., Petravick, D., Pier, J. R., Pope, A., Pordes, R., Prosapio, A., Rechenmacher, R., Quinn, T. R., Richards, G. T., Richmond, M. W., Rivetta, C. H., Rockosi, C. M., Ruthmansdorfer, K., Sand ford, D., Schlegel, D. J., Schneider, D. P., Sekiguchi, M., Sergey, G., Shimasaku, K., Siegmund, W. A., Smee, S., Smith, J. A., Snedden, S., Stone, R., Stoughton, C., Strauss, M. A., Stubbs, C., SubbaRao, M., Szalay, A. S., Szapudi, I., Szokoly, G. P., Thakar, A. R., Tremonti, C., Tucker, D. L., Uomoto, A., Vanden Berk, D., Vogeley, M. S., Waddell, P., Wang, S.-i., Watanabe, M., Weinberg, D. H., Yanny, B., Yasuda, N., & SDSS Collaboration (2000). The Sloan Digital Sky Survey: Technical Summary. *The Astronomical Journal*, 120, 1579–1587.

Zheng, Z., Berlind, A. A., Weinberg, D. H., Benson, A. J., Baugh, C. M., Cole, S., Davé, R., Frenk, C. S., Katz, N., & Lacey, C. G. (2005). Theoretical Models of the Halo Occupation Distribution: Separating Central and Satellite Galaxies. *The Astrophysical Journal*, 633, 791–809.

Zibetti, S., Charlot, S., & Rix, H.-W. (2009). Resolved stellar mass maps of galaxies - I. Method and implications for global mass estimates. *Monthly Notices of the Royal Astronomical Society*, 400, 1181–1198.

Zwicky, F. (1937). On the Masses of Nebulae and of Clusters of Nebulae. *The Astrophysical Journal*, 86, 217.